A new global dataset of mountain glacier centerlines and lengths

Dahong Zhang [1, 2], Gang Zhou [1, 2], Wen Li [1, 2], Shiqiang Zhang [1, 2], Xiaojun Yao [3], Shimei Wei [3]

[1] College of Urban and Environmental Science, Northwest University, Xi'an 710127, PR China

[2] Shaanxi Key Laboratory of Earth Surface System and Environmental Carrying Capacity, Northwest University, Xi'an 710127, PR China

[3] College of Geography and Environment Sciences, Northwest Normal University, Lanzhou 730070, PR China

Correspondence: Shiqiang Zhang (zhangsq@lzb.ac.cn)

Abstract. The length of a glacier is a key determinant of its geometry and is an important parameter in glacier inventories and modeling; glacier centerlines are the lines along which the main flow of glaciers takes place and, thus, are crucial inputs for many glaciological applications. In this study, the centerlines and maximum lengths of global glaciers were extracted using a self-designed automatic extraction algorithm based on the latest global glacier inventory data, digital elevation model (DEM), and European allocation theory. The accuracy of the dataset was evaluated through random visual assessments and comparisons with the Randolph Glacier Inventory (RGI) version 6.0. A total of 8.25% of the outlines of the RGI were excluded, including 10,764 erroneous glacier polygons, 7,174 ice caps, and 419 nominal glaciers. A total of 198,137 glacier centerlines were generated, accounting for 99.74% of the input glaciers. The accuracy of glacier centerlines was 89.68%. A comparison between the dataset and the previous dataset suggested that most glacier centerlines were slightly longer than those in RGI v6.0, meaning that the maximum lengths of some glaciers had been likely underestimated in the past. The constructed dataset comprises 17 sub-datasets, including global glacier centerlines, maximum lengths, and DEMs, all of which can be found at: https://doi.org/10.11922/sciencedb.01643 (Zhang and Zhang, 2022).

1 Introduction

Mountain glaciers are shrinking rapidly (Hugonnet et al., 2021), altering regional hydrology (Pritchard, 2019), raising global sea levels (Cazenave, 2018), and increasing the risk of natural hazards (Shukla and Sen, 2021; Zheng et al., 2021), and are among the most climate-sensitive constituents of the world's natural water towers (Immerzeel et al., 2019). Under the influence of global climate change, studies on glacier area changes (Sommer et al., 2020; Li et al., 2021), ice thickness (Farinotti et al., 2019), mass balance (Zemp et al., 2019; Vargo et al., 2020; Wu et al., 2021; Mankoff et al., 2021), ice velocity field (Thogersen et al., 2019; Solgaard et al., 2021; Franke et al., 2022), the impact of debris-cover (Scherler et al., 2018; Shukla et al., 2020; Herreid and Pellicciotti, 2020), glacier meltwater (Noel et al., 2020), sediment release (Aciego et al., 2015; Li et al., 2019), and related hazards (Zhou et al., 2021b; Stuart-Smith et al., 2021; Kääb et al., 2021) are essential for global water resources supply assessment and disaster prevention and reduction.

The most noticeable distinction between glaciers and other natural ice bodies is their property of moving towards lower altitudes under the influence of gravity. Glacier flow lines correspond to a glacier's motion trajectories, and the main flow line is the key trajectory. Due to the lack of glacier velocity field data, the main flow lines cannot be obtained on a large scale. The glacier centerline, generated via the axis line method (Le Bris and Paul, 2013; Machguth and Huss, 2014; Kienholz et al., 2014; Zhang et al., 2021), is typically used to represent the main flow line. The glacier centerline

44   is a critical parameter for analyzing the ice velocity field (Heid and Kääb, 2012; Melkonian et al.,
45   2017), estimating glacier volumes (Li et al., 2012; Gao et al., 2018), and developing glacier models
46   (Oerlemans, 1997; Sugiyama et al., 2007; Maussion et al., 2019).

47

48   Glacier length, usually refers to the maximum length of a glacier centerline (main flow line) and
49   represents the longest motion trajectory of a glacier, which is among the key determinants of glacier
50   geometry and a basic parameter of glacier inventories (RGI Consortium, 2017) and modeling
51   (Maussion et al., 2019). Glacier length fluctuations can be used to quantify glacier changes (Zhou
52   et al., 2021a), such as by identifying glacier advancement, surge, or retreat. Glacier length
53   fluctuations (e.g., Leclercq et al., 2014) have also been used to study the relationships with changes
54   in glacier area (Winsvold et al., 2014) and the geometric structure of a glacier (Herla et al., 2017),
55   estimate glacier volume in combination with the glacier area (Lüthi et al., 2010), and reconstruct
56   annual averaged surface temperatures over the past 400 years on hemispherical and global scales
57   (Leclercq and Oerlemans, 2011).

58

59   A complete global inventory of glacier outlines (RGI Consortium, 2017) was created following the
60   Fifth Assessment Report of the Intergovernmental Panel on Climate Change (IPCC AR5). Three
61   types of automatic and semi-automatic methods have been proposed to meet the demand for large-
62   scale acquisitions of glacier lengths. First, there are typical hydrological analysis methods (Schiefer
63   et al., 2008), but they result in lengths that are longer than equivalent maximum distances taken
64   along typical longitudinal centerline profiles. The second type is a simplified algorithm based on
65   the skeleton theory (Le Moine and Gsell, 2015), but it has not been widely used. Third, there are
66   centerline methods based on the axis concept proposed by Le Bris and Paul (2013) and first applied
67   to calculating global glacier length by Machguth and Huss (2014). However, with this type of
68   algorithm, the glacier centerlines tend to be noticeably deflected by their tributaries (Le Bris and
69   Paul, 2013). The cost grid-least-cost route approach of Kienholz et al. (2014) based on the axis
70   concept is more accurate but also more labor and time-consuming, which limits its application to
71   global glaciers. The trade-off function approach of Machguth and Huss (2014), which is based on
72   the axis concept, has been applied to almost all global mountain glaciers but excludes the centerlines
73   of the branches of glaciers. Despite many attempts to overcome these limitations in recent years
74   (Yao et al., 2015; Yang et al., 2016; Ji et al., 2017; Hansen et al., 2020; Xia, 2020; Zhang et al.,
75   2021), to date, global datasets of the centerline and length of mountain glaciers are rare. Based on
76   our recent study on successfully extracting the glacier centerline using the Euclidean allocation
77   method (Zhang et al., 2021), we aim to combine publicly available digital elevation data into one
78   global digital elevation model (DEM) at 30-m resolution and extending from 90°N to 90°S, to check
79   and correct the global glacier outlines and obtain a new graphic dataset of the centerline and length
80   of global mountain glaciers.

81

82   **2 Study region and data**
83   The glacier dataset used in this study was the Randolph Glacier Inventory version 6.0 (RGI v6.0)
84   (http://www.glims.org/RGI/randolph.html, last accessed: 15 November 2021) released via the
85   Global Land Ice Measurements from Space initiative (GLIMS), which is a globally complete
86   collection of digital glacier outlines, excluding ice sheets (Pfeffer et al., 2014). RGI v6.0 includes
87   216,502 global glaciers (215,547 glaciers described in the product handbook), with a total area of

88 705,738.793 km² (RGI Consortium, 2017). All glaciers can be divided into 19 first-order glacier

89 regions (Radić and Hock, 2010), which were used in our study (Fig. 1).

90
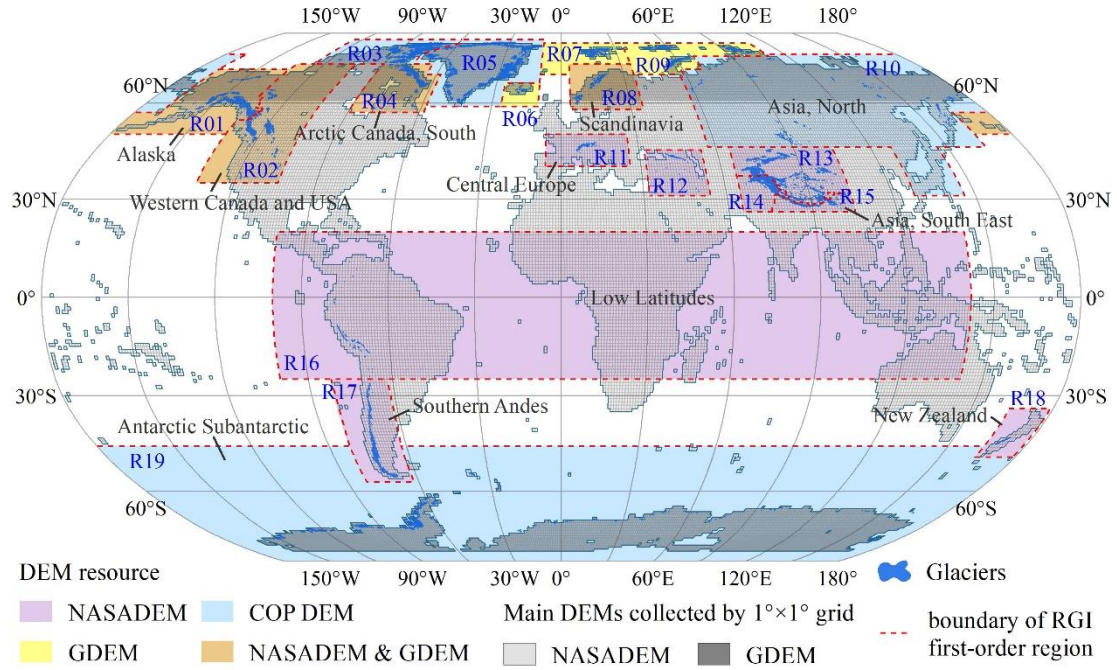
91 **Figure 1.** Distribution of global glaciers, first-order glacier regions, and Digital Elevation Models
92 (DEMs) used. The background is the global DEM grid (1°×1°) covered by NASADEM and GDEM.
93 GDEM and COP DEM represent the ASTER GDEM v3 and the Copernicus DEM, respectively.
94 **Notes:** R01: Alaska; R02: Western Canada and USA; R03: Arctic Canada, North; R04: Arctic
95 Canada, South; R05: Greenland Periphery; R06: Iceland; R07: Svalbard and Jan Mayen; R08:
96 Scandinavia; R09: Russian Arctic; R10: North Asia; R11: Central Europe; R12: Caucasus and
97 Middle East; R13: Asia, Central; R14: Asia, South West; R15: South Asia East; R16: Low Latitudes;
98 R17: Southern Andes; R18: New Zealand; R19: Antarctic Subantarctic.

99

100 Five DEM products (Table 1) were used in this study. The National Aeronautics and Space
101 Administration (NASA) DEM (NASADEM) (https://lpdaac.usgs.gov/news/release-nasadem-data-
102 products/, last accessed: November 17, 2021) was released by the Land Processes Distributed Active
103 Archive Center (LP DAAC) in January 2020. NASADEM is the reprocessed version of the NASA
104 Shuttle Radar Topography Mission (SRTM) data (Farr et al., 2007), with a low mean absolute error
105 (MAE) (Carrera-Hernández, 2021) and improved root mean square error (RMSE) (Uuemaa et al.,
106 2020). Serving the zonal extent of (56°S, 61°N), NASADEM was used as the preferred DEM in this
107 study because of its superior performance. The Advanced Spaceborne Thermal Emission and
108 Reflection Radiometer (ASTER) is a 14-channel imaging instrument operating on the Terra satellite
109 of NASA since 1999. The ASTER Global Digital Elevation Model (GDEM) version 3
110 (https://lpdaac.usgs.gov/news/nasa-and-meti-release-aster-global-dem-version-3/, last accessed:
111 November 17, 2021) (Abrams et al., 2020) was released by Japan's Ministry of Economy, Trade,
112 and Industry (METI) and NASA in July 2019. Using ICESat data, Carabajal and Boy (2016) found
113 that ASTER GDEM v3 displayed smaller means, similar medians, and less scatter than the ASTER
114 GDEM v2 in Greenland and Antarctica. ASTER GDEM v3 was used as the second priority DEM
115 to cover the zonal extents of (56°S, 83°S) and (61°N, 83°N).

NASADEM and ASTER GDEM v3 do not cover all glacierized regions, missing parts of the polar regions and the Kamchatka Peninsula. Because of their high temporal and spatial resolutions at high latitudes, the Reference Elevation Model of Antarctica (REMA) (Howat et al., 2019) and ArcticDEM (https://www.pgc.umn.edu/data/arcticdem/, last accessed: November 17, 2021) were preferred as the supplementary data of our preliminary studies in these glacier regions. Nevertheless, ArcticDEM and REMA were found to be inadequate because of insufficient coverage and sporadic data. Some other DEMs in high latitude areas (Fan et al., 2022; Zhang et al., 2022) were also not considered because their spatial resolutions are very different from that required in this study. Therefore, the wide-coverage Copernicus DEM (https://spacedata.copernicus.eu/web/cscda/cop-dem-faq, last accessed: November 17, 2021) was finally selected as the supplementary dataset for glacier regions not entirely covered by NASADEM and ASTER GDEM v3. The Copernicus DEM was released in November 2020. The accuracy assessment undertaken by its development team (the product handbook) using TanDEM-X DEM/World DEM ICESat GLAS reference points found an absolute vertical accuracy of approximately 10 m at the periphery of Antarctica and Greenland. In summary, NASADEM, ASTER GDEM v3, and Copernicus DEM were compiled to create a 30-m DEM that covered the study area completely.

Table 1. All DEMs collected in this study

DEM	Extent	Resolution	Access
NASADEM	[56°S, 61°N]	30 m	https://search.earthdata.nasa.gov/search
ASTER GDEM v3	[83°S, 83°N]	30 m	https://gdemdl.aster.jspacesystems.or.jp/
ArcticDEM	[55°N, 90°N]	2 m	https://earthengine.google.com/
REMA	[60°S, 88°S]	2m / 8m	https://earthengine.google.com/
Copernicus DEM	Global	30 m	https://panda.copernicus.eu/web/cds-catalogue/panda

Note: The interval in the 'Extent' column represents all landmasses within the zonal range, although not all areas within the range may be covered.

In addition, graphical data (Machguth and Huss, 2014) of glacier length in *. xy format (the UTM projection), which correspond to the attribute of the glacier maximum length (L_{max}) in RGI v6.0, were collected in High Asia. Because these data were obtained from an unofficial source, we could not access their documentations and recovered only the coordinates of points matching some of the glaciers in RGI v6.0. The registration of the *. xy file depends on matching its filename with the feature identity document (FID) of the glacier polygon of RGI v6.0 in the same glacier area. The glacier lengths (*MHMLDS*) of successful registration were used as graphical validation data for this study.

3 Methods

3.1 Outline of workflow

This study relied on two key input datasets: the global glacier inventory and the compiled global glacier elevation. An outline of the workflow for establishing a new dataset of global graphic glacier centerlines and lengths is shown in Figure 2. The process was divided into six parts: (1) design an algorithm to check all glacier outlines and exclude defective glacier polygons; (2) buffer glaciers to produce a mask containing global glaciers and their buffers; (3) mosaic the compiled global DEMs according to the mask in step 2 to prepare the global glacier elevation data; (4) determine the automatic extraction parameters of global glacier centerlines by repeated testing in each region; (5)

155   input the global DEM, glacier outline dataset, and all parameters into the designed automatic
156   extraction software (Zhang et al., 2021) to generate global centerlines and lengths; and (6) verify
157   and compare with existing centerline results to evaluate the accuracy of the new datasets.

158
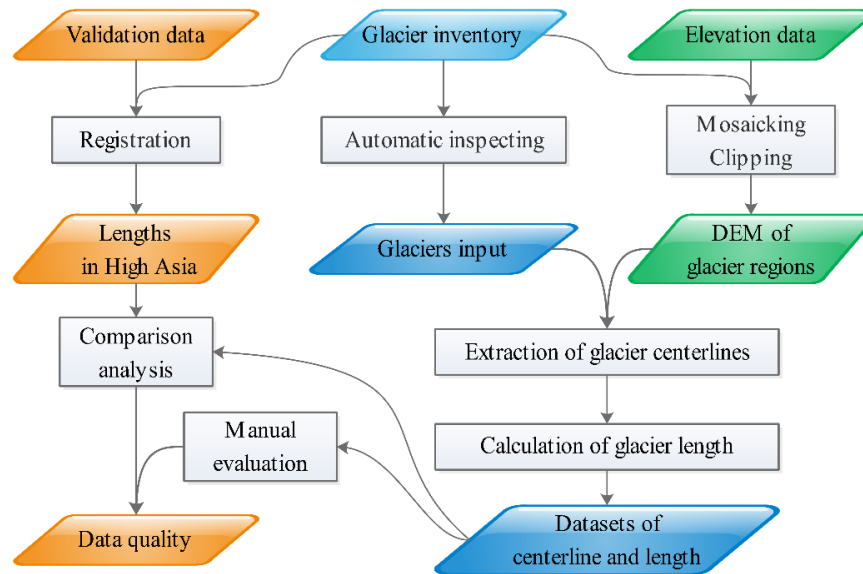
159   **Figure 2.** Workflow of the centerline and length dataset production.

160

161   **3.2 Illustration of key methods**

162   **3.2.1 Pre-processing of glacier outlines**

163   This study had strict requirements for glacier outlines and, therefore, all glacier complexes were

164   divided into individual glaciers prior the centerline extraction. However, because of the limited

165   semi-automatic glacier segmentation approach (Kienholz et al., 2013) and the high-priority strategy

166   of completeness of coverage adopted by RGI v6.0 (RGI Consortium, 2017), some glaciers were not

167   supported by our algorithm. These unsupported glaciers included three categories: glacier

168   complexes with/without inaccurate segmentation (Fig. 3a-b), erroneous glacier outlines (Fig. 3c)

169   resulting from the vectorization, and flawed glaciers (Fig. 3d-f) generated by the automatic

170   extraction algorithm. For the third category, we designed an identification algorithm to mark and

171   screen them (described in the last paragraph of this section). The flaws in these glacier outlines were

172   mainly caused by topological errors of polylines/polygons, such as unclosed, sawtooth, and

173   overlapping polygons. The first two categories did not affect the algorithm's normal operation;

174   however, the extraction accuracy is not always guaranteed. We could not identify the source of the

175   problem at the time of the study, and a solution is needed to improve the quality of the global glacier

176   inventory.
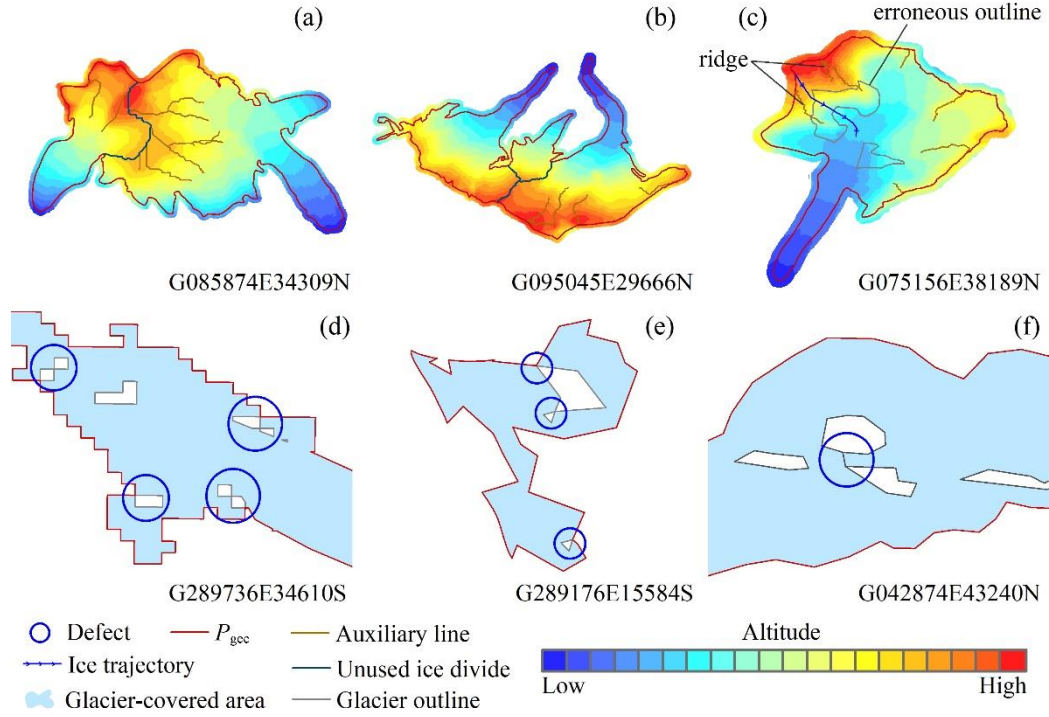
Figure 3. Schematic of three types of flawed glacier outlines. **(a-b)** Glacier complexes with/without inaccurate segmentation. **(c)** Erroneous glacier outline caused by vectorization. **(d-f)** Common problems in flawed glaciers: defects in the automatic algorithm, defects in post-processing, and artificial errors. The auxiliary line represents lower-grade ice divides in an individual glacier, which is part of the ridge lines.

In this study, we defined the external contour of a glacier (P_{gec}), namely, the polygon corresponding to the longest closed polyline of the glacier, to reduce the storage of DEMs and improve the efficiency of batch processing. The buffer masks of all glaciers (buffer distance: approximately 100 m) were generated by their P_{gec} to meet the requirement for the extent of input DEMs to be slightly larger than the P_{gec}. The buffer masks generated initially were partially broken because there were overlaps or gaps between adjacent polygons of the buffer zone; thus, polygons with a perimeter of less than 12 times the buffer mask distances of each region were removed.

The third category of flawed glaciers (Fig. 3d-f) was identified by obtaining P_{gec}. The most common error type was a glacier outline with two or more closed polylines with the same endpoint. These flawed glacier outlines were identified by assessing whether there were multiple polylines sharing endpoints after converting the glacier from a polygon to a polyline. However, these outlines did not include the unclosed types: a few glacier outlines that appeared to be closed polylines, but had geometric flaws such as non-coinciding head and tail endpoints of the polylines.

3.2.2 Preparation of input datasets

All the data associated with the dataset production were processed in units of first-order glacier regions. The input glacier outlines excluded all the defective glacier outlines. Similarly, the nominal glaciers (represented by an ellipse) and ice caps remarked in RGI v6.0 were also treated, which were distinguished by two attributes: status (nominal glacier) and form (ice cap). The inspection of glacier

outlines show that there are 10,764 defective glacier outlines (*FGODS*) in RGI v6.0, accounting for approximately 4.97% of the total (216,502) (Table 2). After excluding nominal glaciers (461) and ice caps (7,174), 198,646 glaciers remained as input glacier outlines (*IGODS*), accounting for 91.75% of the global mountain glaciers.

Table 2. Preprocessing results of different glacier regions and information of input datasets.

Region	Region Name	Total	Ice Cap	Nominal glacier	Flawed glacier	Glacier input	DEM input
R01	Alaska	27108	0	0	704	26404	NASADEM, GDEM
R02	Western Canada and USA	18855	0	0	1564	17291	NASADEM, GDEM
R03	Arctic Canada, North	4556	650	0	47	3869	COP DEM
R04	Arctic Canada, South	7415	953	0	63	6409	NASADEM, GDEM
R05	Greenland Periphery	20261	1658	0	1547	17247	COP DEM
R06	Iceland	568	133	0	1	435	GDEM
R07	Svalbard	1615	144	0	12	1460	GDEM
R08	Scandinavia	3417	0	4	75	3338	NASADEM, GDEM
R09	Russian Arctic	1069	460	0	0	609	GDEM
R10	North Asia	5151	5	116	136	4899	COP DEM
R11	Central Europe	3927	0	2	76	3849	NASADEM
R12	Caucasus Middle East	1888	0	339	2	1547	NASADEM
R13	Central Asia	54429	1545	0	28	52858	NASADEM
R14	South Asia West	27988	295	0	1946	25792	NASADEM
R15	South Asia East	13119	289	0	4	12826	NASADEM
R16	Low Latitudes	2939	0	0	724	2215	NASADEM
R17	Southern Andes	15908	623	0	3828	11734	NASADEM
R18	New Zealand	3537	0	0	0	3537	NASADEM
R19	Antarctic Subantarctic	2752	419	0	7	2327	COP DEM
--	--	216502	7174	461	10764	198646	--

Note: GDEM and COP DEM refer to ASTER GDEM v3 and Copernicus DEM, respectively.

The P_{gec} of all glaciers in RGI v6.0 comprises the global glacier external contour dataset (*GGECDS*), which generated the global mountain glacier's buffer mask dataset (*GGBMDS*). The collected DEMs were extracted using *GGBMDS* and 43,035 DEM tiles were generated. They were then mosaicked according to different first-order glacier regions to generate a global glacier elevation dataset (*GGEDS*). The details of the two input datasets are presented in Table 2.

3.2.3 Generation of centerline and glacier length

Glacier centerlines and length were automatically extracted with the 'GlacierCenterlines_Py27' (Update to version 5.2.1) tool, which is based on the axis concept and Euclidean allocation (Zhang et al., 2021). The principle is briefly explained as follows: the highest and lowest points of the external outline of a glacier were extracted as two endpoints that divide the glacier outline into two parts; In the glacier polygon, points that have the equal shortest distances to the two parts were identified as other vertices; The line formed by two endpoints and these other vertices was regarded as the glacier centerline. The maximum length of glaciers was calculated using an algorithm similar to the critical path. The updated contents focused on formulating the parameterization scheme (Appendix A: Table A1) for extracting global glacier centerlines, as well as repairing some newly discovered bugs, such as a dead cycle in the process of auxiliary line extraction. All glacier outlines included in the *IGODS* were divided into ten levels based on the proportion of cumulative area after ranking the area of all input glacier polygons from small to large (Table 3). The Albers projection (See Supplement for detailed parameter files) with WGS1984 was used as a unified projection

coordinate system for each glacier region. The empirical values of the other parameters were determined in repeated attempts, and their values were significantly correlated with the glacier scale. The generated glacier centerlines were merged according to the glacier regions. Then, the graphics and attribute information of glacier length were exported as corresponding independent ESRI shapefiles. In addition, other data associated with the dataset production were exported, such as the segmentation results of glacier outlines, the lengths in the accumulation and ablation region of each glacier, the lowest points, the local highest points (P_{max}), the extracted failed glacier outlines, and logs.

Table 3. Global glaciers stratified by area.

Level	Count	Area/km^2	Acc. area/km^2	Percent	Interval/km^2
L1	165593	1.00	41313.79	10%	[0.01, 1.00]
L2	22833	3.57	82629.47	20%	(1.00, 3.57]
L3	6906	11.39	123947.69	30%	(3.57, 11.39]
L4	2149	35.51	165282.14	40%	(11.39, 35.51]
L5	698	103.10	206631.32	50%	(35.51, 103.10]
L6	262	248.26	247917.55	60%	(103.10, 248.26]
L7	113	521.40	289227.71	70%	(248.26, 521.40]
L8	55	1087.47	330595.34	80%	(521.40, 1087.47]
L9	27	2657.74	374312.14	90%	(1087.47, 2657.74]
L10	10	6004.85	413136.71	100%	(2657.74, 6004.85]
Total	198646	--	--	--	--

3.2.4 Accuracy assessment

A random assessment was prioritized to assess the accuracy of the extracted centerlines. We randomly selected 100 glaciers in each of the 19 glacier regions, obtaining a total of 1,900 glacier centerlines (N_G). These glacier centerlines were divided into three first-level categories (Zhang et al., 2021): correct (I), inaccurate (II), and incorrect (III). Type II mostly contained glaciers with accurate glacier maximum lengths but missing, redundant, or unreasonable branches of glacier centerlines. When calculating the dataset accuracy, Types I and II were regarded as correct, and only Type III was considered incorrect. Finally, the proportion of Type III glaciers in the sample was counted, and the valuation result (R) was calculated using Eq. (1):

$$R = \sum_{i=1}^{19} \frac{S_i \times N_{T_i}}{N_G} \qquad , (1)$$

where N_G is the total number of glaciers centerlines and N_{Ti} and S_i are the verification accuracy and the number of glaciers in the i th glacier region ($i = 1, 2, 3, ..., 18,19$), respectively.

This study's maximum glacier lengths (G_{Lmax}) were compared with the L_{max} (Machguth and Huss, 2014) in RGI v6.0 using linear correlation and ratio analysis. The correlations between G_{Lmax} and L_{max} were established according to different glacier regions, and glacier levels, and the length ratio R_r (Eq. 2) was calculated:

$$R_r = \frac{G_{Lmax}}{L_{max}} \qquad (2)$$

In addition, considering the differences between the graphics, we also collected graph data of glacier length extracted by Machguth and Huss (2014). Considering the limited availability of the data

(obtained: R13–R15), we only compared two glacier-covered regions in the Himalayas: Mount Qomolangma and Kangchenjunga (the world's third-highest mountain) and their surrounding areas.

4 Results

4.1 Centerline and length of glaciers

Taking the *IGODS*, *GGEDS*, and other model parameters (Appendix A: Table A1) as input data, 198,137 glacier centerlines were automatically generated using the centerline extraction tool of 'GlacierCenterlines_Py27 v5.2.1', with an overall success rate of 99.74%. The number and proportion of flawed glacier outlines, nominal glaciers, ice caps, input glacier outlines, and extraction results for distinct glacier regions are shown in Fig. 4.
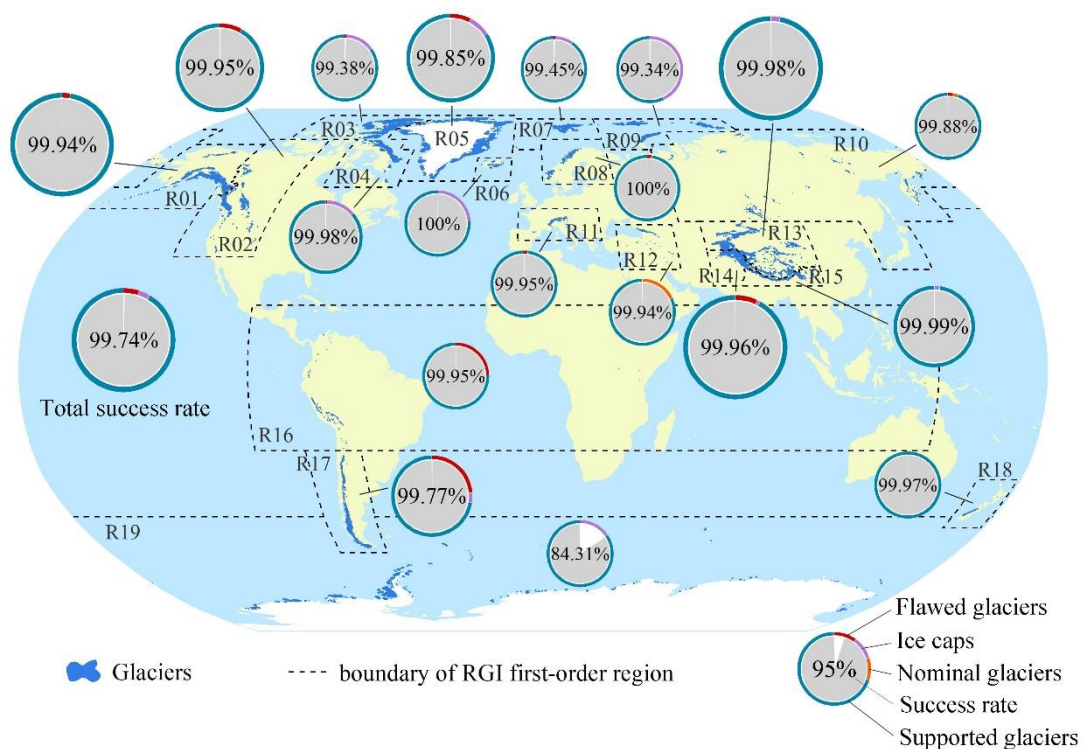
Figure 4. Extraction of glacier centerlines in different glacier regions. The pie chart rings indicate the proportions of input glaciers and of the three types of excluded glaciers in the region. The pie chart represents the correct rate, which is the proportion of correctly extracted glaciers. The size of the pie/ring represents the grade of the glaciers in the region.

Except for Antarctica and Subantarctica (R19), the success rate of extracting glacier centerlines in other glacier regions was greater than 99%, which indicates that the automatic extraction algorithm for glacier centerlines is robust. A small number of glacier outlines with falsely closed boundaries and unidentified ice caps were the main reasons for the failure of the automatic extraction of glacier centerlines; however, it is difficult to establish rules for accurately identifying these glacier polygons. In total, 510 unsuccessful glacier outlines were identified, of which Antarctic-Subantarctic (R19) accounted for 71.57%; Southern Andes (R17) and Greenland Periphery (R05) for 5.29% and 5.1%, respectively; Arctic Canada North (R03) and Alaska (R01) for 4.71% and 2.94%, respectively; and other glacier regions for less than 2%.

Overall, the global glacier centerline dataset (*GGCLDS*) constructed in this study contained 91.52% of the total glaciers in RGI v6.0. The lengths of each branch of the glacier centerline were derived and the longest branch lengths of the glacier centerline were defined as the glacier maximum length (G_{Lmax}), which were used to form the global glacier maximum length dataset (*GGMLDS*). The average centerline length of all branches of a glacier is called the glacier mean length (G_{Lmean}). In addition, the median glacier altitude was regarded as the equilibrium line altitude (ELA) (Machguth and Huss, 2014). The part with G_{Lmax} higher than ELA was regarded as the length of the glacier accumulation zone (G_{Lacc}), and the part lower than ELA was regarded as the length of the glacier ablation zone (G_{Labl}), which formed the glacier accumulation zonal length dataset (*GACLDS*) and glacier ablation zone length dataset (*GABLDS*). The key process data corresponding to *GGCLDS* were also output, to form the glacier outline segmentation results (*GOSRDS*), lowest points (*GGLPDS*), local highest points (*GLHPDS*), and unsuccessful glacier outlines (*GUGODS*). The fields involved in all datasets are listed in Table 4.

Table 4. Description of the attributes contained in all datasets.

Name	Data type	Char. length	Description
GLIMS_ID	Char.	14	Unique code of a glacier
Type	Long int.	4	Glacier grade in this study
MaxL	Float	8	Glacier maximum length (Unit: m)
MeanL	Float	8	Glacier average length (Unit: m)
ELA	Long int.	4	Equilibrium line altitude (Unit: m)
AccL	Float	8	Length in the accumulation region (Unit: m)
AblationL	Float	8	Length in the ablation region (Unit: m)
Id	Long int.	8	Data code of the same glacier
BS	Long int.	8	Tag of the same segment in a glacier
RASTERVALU	Long int.	4	Altitude of a P_{max} (Unit: m)

Note: Char.: Character; int.: integer.

The glacier outlines of RGI v6.0 without centerlines obtained in this study were limited by the quality of the glacier polygons, which mainly correspond to the flawed glacier outlines *(FGODS)*, and the identified ice caps in RGI v6.0 (Table 2). Among the *FGODS* (10,764), Southern Andes (R17) had the most, followed by Southwest Asia (R14); Western Canada and USA (R02) and Greenland Periphery (R05), with slightly more than 1,500; and Low Latitudes (R16) and Alaska (R01), with slightly more than 700. There were 451 in other glacier regions, including two regions with 0 defective glacier outline, the Russian Arctic (R09) and New Zealand (R18). Among the ice caps (7174) identified by RGI v6.0, slightly more than 1,500 were in R05 and Central Asia (R13), between 500 and 1,000 in the Arctic Canada South (R04), Arctic Canada North (R03), and R17, and less than 500 in other glacier regions. Nominal glaciers (461) existed in three glacial regions: Caucasus Middle East (R12), North Asia (R10), and Scandinavia (R08).

4.2 Data validation
4.2.1 Random assessment results
The evaluation results using random samples from the glacier centerline dataset suggested that the average verification accuracy of the glacier centerline dataset was 89.68%. There were significant differences across the accuracies of the 19 glacier regions around the world (Fig. 5). Among them, R11, R15 and R10, R09, and R19 had the highest (98%), second highest (95%), second lowest (78%), and lowest (50%) accuracies, respectively. In terms of types, the average proportions of Types I and II were 83.53% and 6.16%, respectively. The proportions of Type I in R07 and R09

were relatively low, at 79% and 73%, respectively, and the lowest in R19 was only 50%. Type II had the highest proportion in R19 at 16%, followed by R07 (10%). Moreover, Type II accounted for more than 5% in seven regions: R11, R13, R17, R18, R16, R01, and R06.
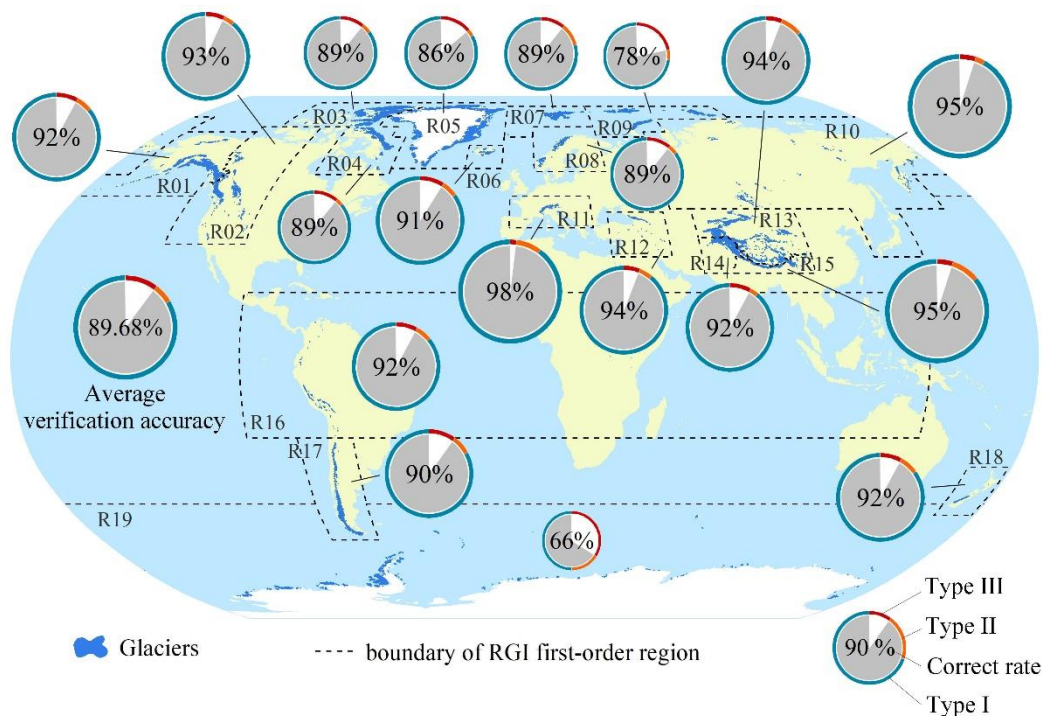
Figure 5. Statistical chart of random evaluation results. The pie chart rings show the proportion of each type with the total number of samples in the region. The pie chart shows the correct rate, which is the proportion of Types I and II in each region. The size of the pie/ring represents the grade of the correct rate in the region. Types I, II, and III (See Section 3.2.4) are correct, inaccurate, and incorrect centerlines, respectively.

The above results indicate that, in addition to the three glacier regions of R07, R09, and R19, the random samples of the glacier centerline dataset show excellent performance in terms of accuracy, particularly in R02, R12, and R14. The unmarked ice cap and local low-quality DEM were the main reasons for the poor quality of the glacier centerlines in R07 and R09. Owing to glacier complexes and low altitude differences in low-quality DEMs at the glacier tongues, glacier centerlines obtained in R19 were of poor quality, but were included for completeness.

4.2.2 Comparison with previous results

We compared the glacier lengths (G_{Lmax}) automatically obtained in this study with those (L_{max}) obtained by Machguth and Huss (2014) (Fig. 6). After eliminating 5408 glaciers with L_{max} value of -9 (missing value), the length values of the other 192,728 glaciers in the global glacier length dataset were compared directly. The G_{Lmax} and L_{max} were generally comparable (Fig. 6a). The glaciers in grades L_4–L_{10} showed excellent agreement, while those of L_1–L_3 determined the linear correlation coefficient owing to their large number. There were approximately 35,000 glaciers with a length ratio (R_r) between G_{Lmax} and L_{max} greater than 1.55, and these were excluded from the histogram in Fig. 6b because there was a high probability that the length of at least one of the two datasets was wrong. The peak value of the histogram of R_r is in the interval 1.05–1.15 and R_r in the interval 0.95–

1.25 accounts for 64.55% (Fig. 6b). The glacier length G_{Lmax} determined in this study was generally 10% longer than L_{max}, which suggests that the glacier centerline lengths were probably underestimated in previous studies. In addition, the length ratio of glacier L_1 was the highest and the median value was high (Fig. 6c). The R_r values of glaciers $L_4–L_{10}$ fluctuated greatly. The R_r distributions of glaciers L_2 and L_3 were relatively concentrated. The reason for this is that the length of glacier L_1 was affected by the DEM, while glaciers $L_4–L_{10}$ were mainly impacted by differences in glacier scale and the accuracy of the auxiliary line.
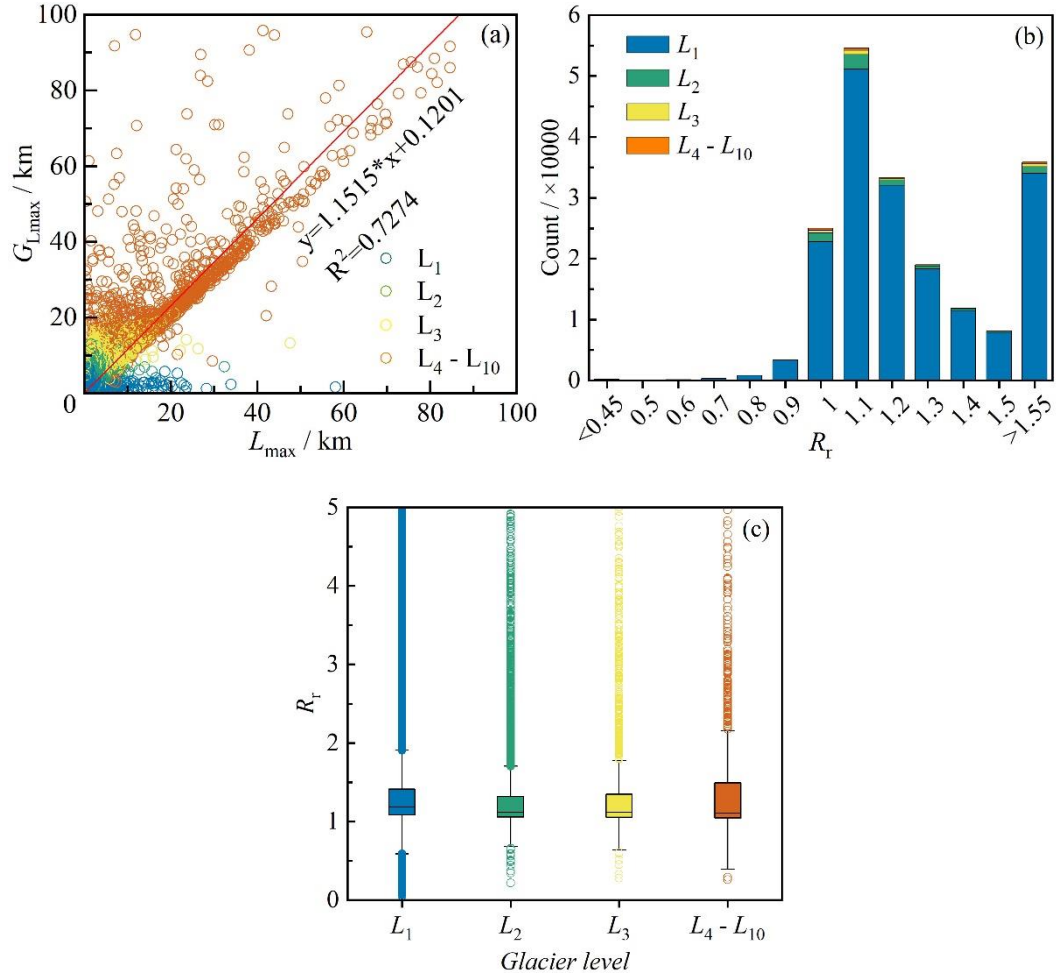
Figure 6. Comparison between longest centerlines calculated in this study and by Machguth and Huss (2014). **(a)** Linear regression of maximum length for all input glaciers (*IGODS*), determined as G_{Lmax} calculated in this study and L_{max} obtained in Machguth and Huss (2014). **(b)** Histogram of length ratio (R_r, G_{Lmax}/L_{max}) for distinct grades of glaciers. **(c)** Box plots of length ratio (R_r) for different scales of glaciers.

Comparisons between G_{Lmax} and L_{max} for each first-order glacier region and all random samples are shown in Appendix B. The fit between G_{Lmax} and L_{max} was better in seven glacier regions including R01, R04, R07, and R12–R15, in which the R^2 was larger than 0.95 (Fig. B1). The R_r in R17 ($R^2 = 0.8174$), R05 ($R^2 = 0.8136$), and R03 ($R^2 = 0.6311$) were lower, whereas that in R19 ($R^2 = 0.5487$) was the worst. The R^2 values of the other eight glacier regions were between 0.85 and 0.95. The histograms (Fig. B2) suggest that G_{Lmax} and L_{max} fitted well in R04, R06, R07, R09, and R12–R15 because they had recognizable single peak values. The peak values of R03, R05, R17, and R19 were

373   not prominent and the proportion of glaciers with $R_r > 1.55$ was extremely high, further increasing

374   the uncertainty in glacier length estimates in these four regions. R01, R07, R08, R11–R15, and R18

375   performed well in the box plot (Fig. B3), whereas the results for R09 were not good. Moreover, the

376   fit of all random samples was poor (Fig. B1, $R^2 = 0.7547$), the peak value was more prominent (Fig.

377   B2), and the length ratio distribution of glaciers of different grades was relatively scattered (Fig.

378   B3). In general, the glacier lengths of R07 and R12–R15 were the closest, while there were

379   significant differences in R03, R05, R17, and R19.

380

381   Furthermore, the graphic results, which were collected for the maximum length of glaciers in parts

382   of High Asia (Machguth and Huss, 2014), were used to compare with this study's. Two parts of R15

383   were showed, which were Mount Qomolangma and its surrounding area (Fig. 7a) and

384   Kangchenjunga and its surrounding area (Fig. 7b). Visual comparison suggested that the extraction

385   approach used in this study was robust (Fig. 7a) and that its sensitivity to topography was lower

386   than that of Machguth and Huss (2014) (Fig. 7b). Large differences in glacier length extraction

387   schemes are present only in a few glaciers or in certain types of glaciers, such as slope glaciers and

388   ice caps.

389

390   **4.2.3 Uncertainties and possibilities for improvement**

391   Although we compared the two current global length datasets, it is still difficult to accurately

392   characterize the dataset's quality in this study. For glaciers for which centerlines were not provided

393   in this dataset, users need to update the corresponding glacier outlines and could use the automatic

394   extraction tool provided in this study to generate their centerlines, including the defective glacier

395   outlines (*FGODS*), nominal glaciers and ice caps of the RGI v6.0. Specifically, the centerlines of

396   the *FGODS* rely on the glacier outlines that meet the requirements of this study. These glacier

397   outlines include glacier inventory data from other sources or the *FGODS* that were repaired by some

398   algorithm or manual process. Nominal glaciers are similar to *FGODS*, and also require users to

399   obtain corresponding glacier outlines. Automatic approaches to dividing ice caps from glacial

400   complexes into individual glaciers are currently limited, and data users can only use their own

401   criteria to separate the ice caps and then use our tool to generate the centerlines. In addition,

402   prioritizing the coverage of this dataset, we designed a geometry-based algorithm to repair *FGODS*

403   and provided users with their centerlines in the form of a supplementary dataset. Corresponding

404   codes and results can be seen in sub-datasets *CODES* and *SUP_220707*.

405

406   The automatic extraction algorithm in this study is more suitable to single-outlet glaciers,

407   particularly valley glaciers; it is not suitable for ice caps, flat-top glaciers, and tidal glaciers, which

408   tend to be widely distributed in the Antarctic, sub-Antarctic, northern Canadian Arctic, among other

409   areas. In short, the uncertainties in this dataset come probably from the centerlines of some slope

410   glaciers and the ice caps that are not identified in RGI v6.0, or a few centerlines with unpredictable

411   quality due to the input data such as the incorrect glacier polygons, erroneous DEMs. In future work,

412   improved glacier inventories and more accurate DEMs will contribute to improving centerline

413   quality. Furthermore, optimizing the automatic glacier segmentation approach, the DEM-based

414   extraction algorithm of glacier feature lines and the centerline trade-off algorithm will also likely

415   further improve the accuracy of glacier centerlines. In addition, centerline accuracy will probably

416   benefit from further improving the classification type of each glacier in the glacier inventory.

417

418
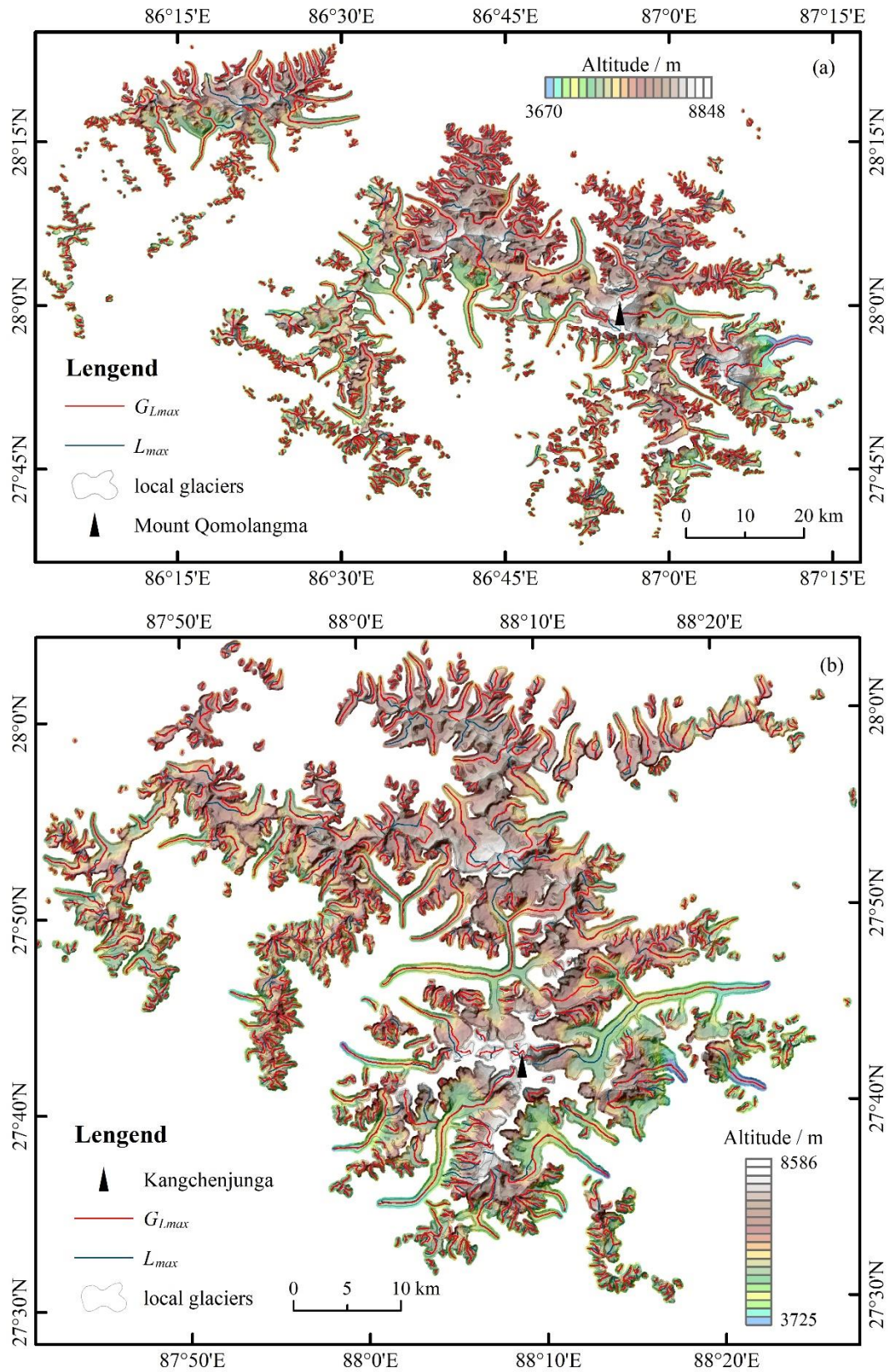
Figure 7. Visual comparison of the longest center lines calculated in this study and by Machguth and Huss (2014) for two glacier-covered regions in the Himalayas, covering Mount Qomolangma (**panel a**) and Kangchenjunga (**panel b**, the world's third highest mountain) and their surrounding areas. In the background is the DEM used for the calculation.

419
420
421
422

5 Data availability

The global glacier centerline dataset (*GGCLDS*), global glacier maximum length dataset (*GGMLDS*), and other relevant datasets are available at https://doi.org/10.11922/sciencedb.01643 (Zhang and Zhang, 2022). All 17 sub-datasets of this dataset are listed in Table 5.

Table 5. Description of the sub-datasets contained in this dataset.

Acronym	Data format	Data volume	Description
IGODS	*.shp	316 MB	Input glacier outline dataset
GGEDS	*.tif	3.70 GB	Global glacier elevation dataset
GGCLDS		838 MB	Global glacier centerline dataset
GGMLDS		616 MB	Global glacier maximum length dataset
GACLDS		302 MB	Global glacier accumulation region length dataset
GABLDS		358 MB	Global glacier ablation region length dataset
GOSRDS		1.16 GB	Global glacier outline segmentation result dataset
GLHPDS		11 MB	Global glacial local highest point dataset
GLPDS	*.shp	6.25 MB	Global glacial lowest point dataset
GUGODS		3.95 MB	Unsuccessful global glacier outline dataset
FGODS		119 MB	Global flawed glacier outline dataset
GGECDS		334 MB	Global glacier external contour dataset
GGBMDS		374 MB	Global glacier buffer mask dataset
MHMLDS		8.32 MB	The maximum length of Machguth and Huss in High Asia
SUP_220707		681 MB	Updated the centerlines of the repaired *FGODS*
CODES	*.py	40 KB	Related codes of data process in bulk
LOGS	*.txt	1.27 MB	Related logfiles of data process in bulk

6 Conclusions

In this study, a new global dataset of glacier centerlines was constructed, and the maximum length was calculated based on the global glacier inventory (RGI v6.0) and global glacier region DEM (*GGEDS*, composed of NASADEM, ASTER GDEM v3, and Copernicus DEM). A total of 198,137 glacier centerlines were generated, accounting for 99.74% of the imported glaciers (*IGODS*) and 91.52% of the global glacier inventory. The overall extraction accuracy of these glacier centerlines (*GGCLDS*) used in random self-assessment was 89.68%. The glacier length (G_{Lmax}) obtained in this study was, on average, approximately 10% longer than that of L_{max}. Nevertheless, our method showed an improved ability to obtain the maximum length, and we believe that the resulting errors were controllable. Furthermore, the preprocessing algorithm we designed accurately identified 10,764 erroneous glacier polygons from RGI v6.0, which formed the defective glacier dataset (*FGODS*).

The global dataset contains 17 sub-datasets, including two basic input datasets (*IGODS* and *GGEDS*), two key result datasets (*GGCLDS* and *GGMLDS*), four process datasets, six derived result datasets, and three supplementary datasets. Ice caps, nominal glaciers, and erroneous glacier polygons were eliminated from most sub-datasets, accounting for approximately 8.25% of the total RGI v6.0. The poor status of these glacier polygons did not support the automatic extraction of glacier centerlines, which needs to be improved in future work. Inevitably, some defects in the algorithm or datasets will also need to be addressed in future research. For instance, the glacial regions (R19 and R03) had the worst results but were nevertheless added to the dataset to prioritize data coverage integrity. The global glacier DEM dataset (*GGEDS*), global glacier external outline dataset (*GGECDS*), and global glacier buffer mask datasets (*GGBMDS*) cover all glaciers in RGI

453 v6.0. Accordingly, they will help design more efficient automated extraction algorithms to produce
454 datasets containing all types of glacier centerlines and lengths worldwide, which is our next goal.
455
456 **Appendix A:** Model parameters resulting from the Central Asia Glacier and extended to worldwide
457 calculations are listed in Table A1.
458 **Table A1.** Parameterization scheme for extracting global glacier centerlines.

Par.	Description	Value (Levels 1-10)	Unit
P_1	Maximum distance between adjacent vertexes	10	m
P_2	Buffer distance outside the glacier outline	30	m
P_3	Threshold of accumulative flow	5 - 8, 10, 20, 30, 50, 100, 200	int $\times 10^3$
P_4	Length of the shortest auxiliary line	10 - 19	int
P_5	Length of the longest auxiliary line	2 - 11	int
P_6	Interval for searching the local highest points	50, 60, 70, 80, 90,100, 200, 300, 400, 500	count
P_7	Matching tolerance of the vertexes of polyline	0.2 ,0.2 ,0.5 ,0.5 ,1 (L_5 - L_{10})	m
P_8	Size of grid cell in Euclidean allocation	1, 5, 15, 15, 30 (L_5 - L_{10})	m
P_9	Minimum distance between the adjacent P_{max}	10, 15, 30, 60, 120, 150, 200, 300, 400, 500	count
P_{10}	Smoothing tolerance of polylines	5, 10, 15, 20, 30 (L_5 - L_{10})	m
P_{11}	Length threshold of the longest auxiliary line	10190	km^2

459 **Notes:** The calculation method for each parameter is detailed in Zhang et al. (2021). P_{max} and L refer to the local
460 highest points and grades of the glacier, respectively.
461
462 **Appendix B:** Comparison between longest centerlines calculated in this study and by Machguth
463 and Huss (2014) for all samples and different first-order glacier regions of RGI v6.0. Linear
464 regression of the two lengths, histogram of length ratio (R_r), and box plots of R_r for glaciers of
465 different grades in these regions were in Figure B1, B2, and B3, respectively.
466

467

468

469

470

471

472

473

474

475
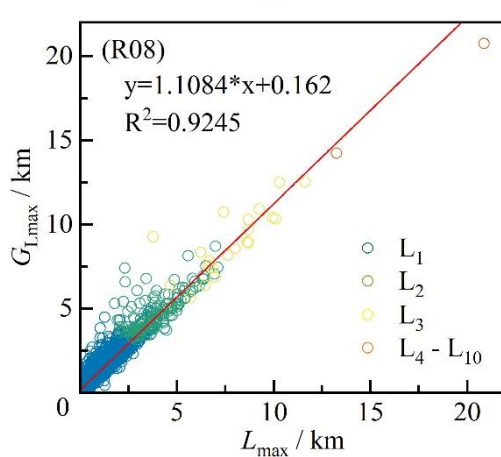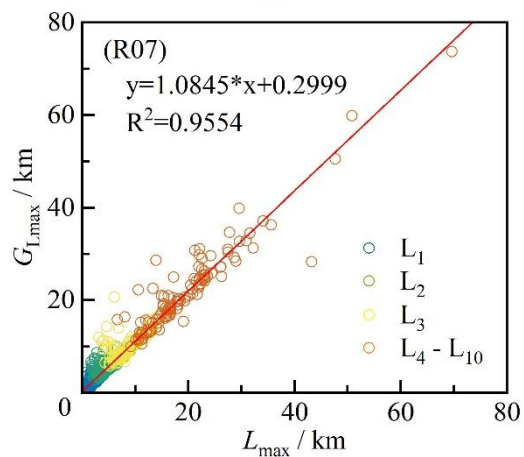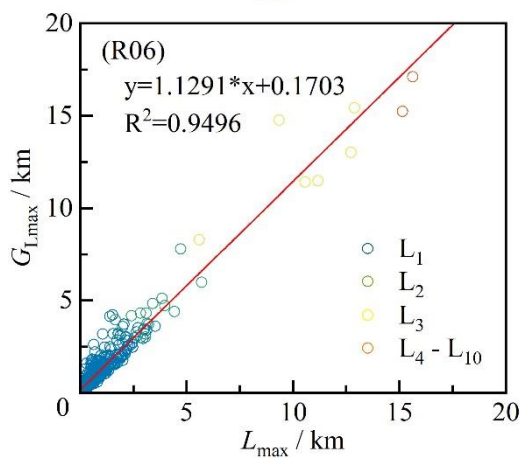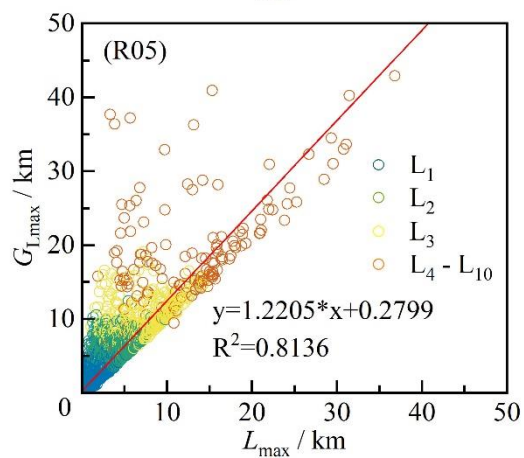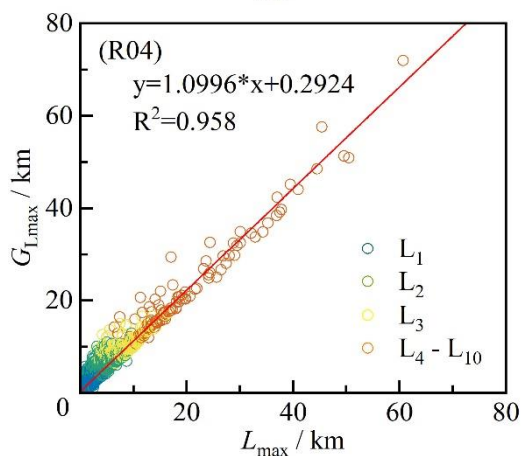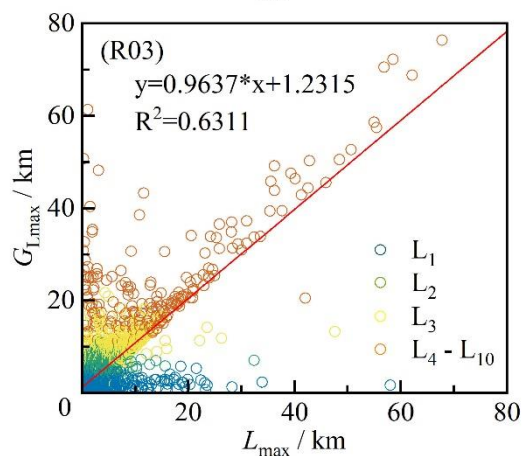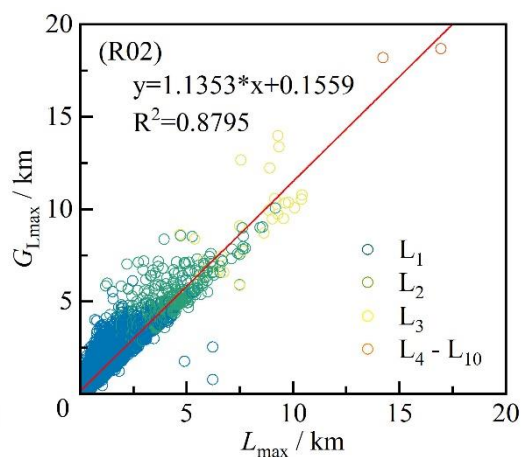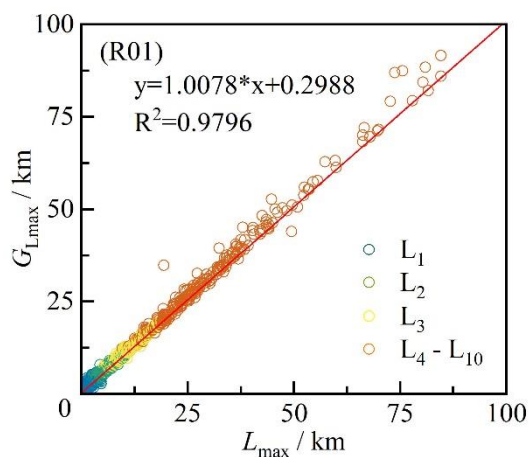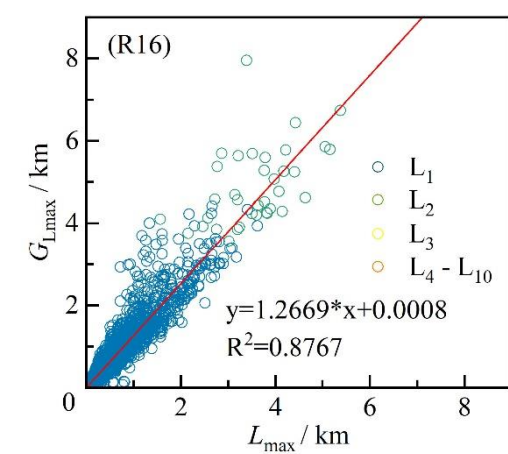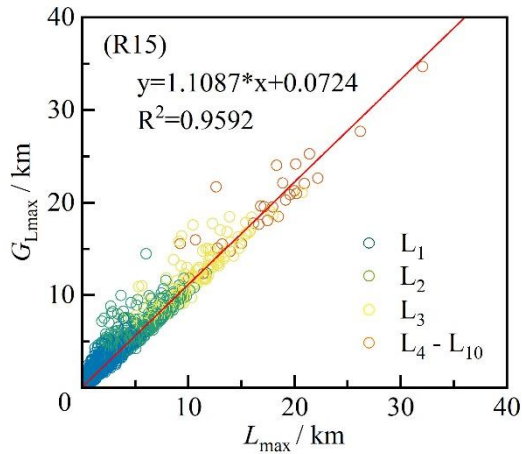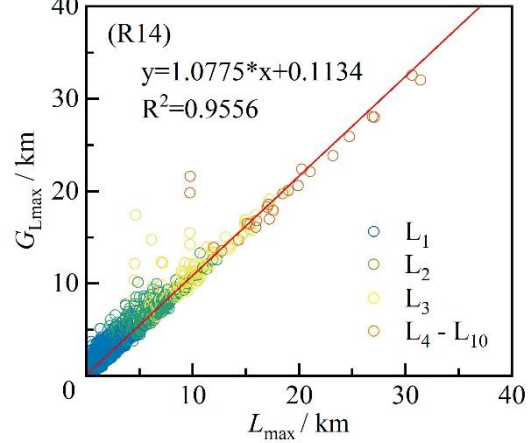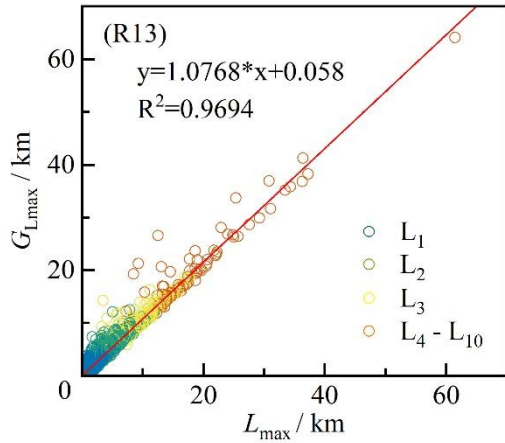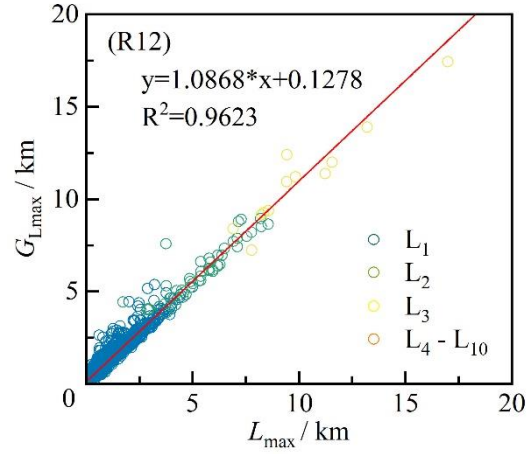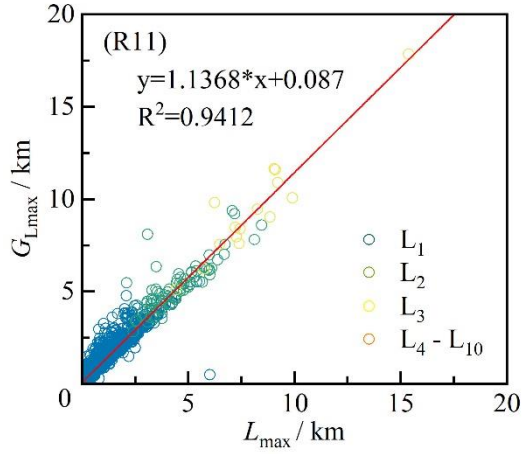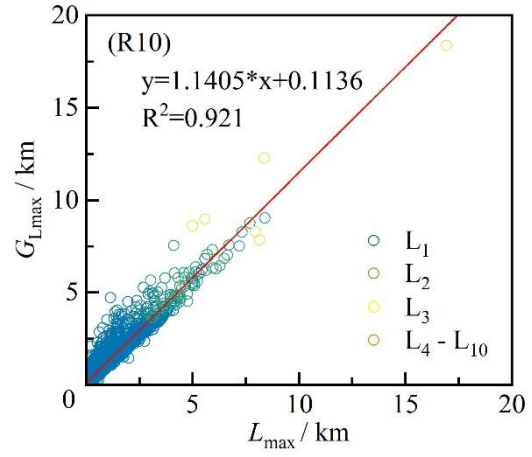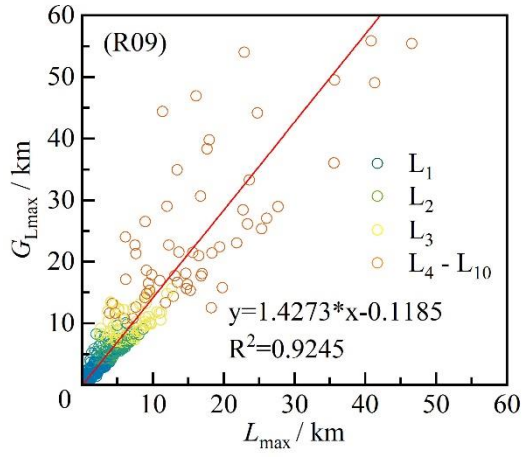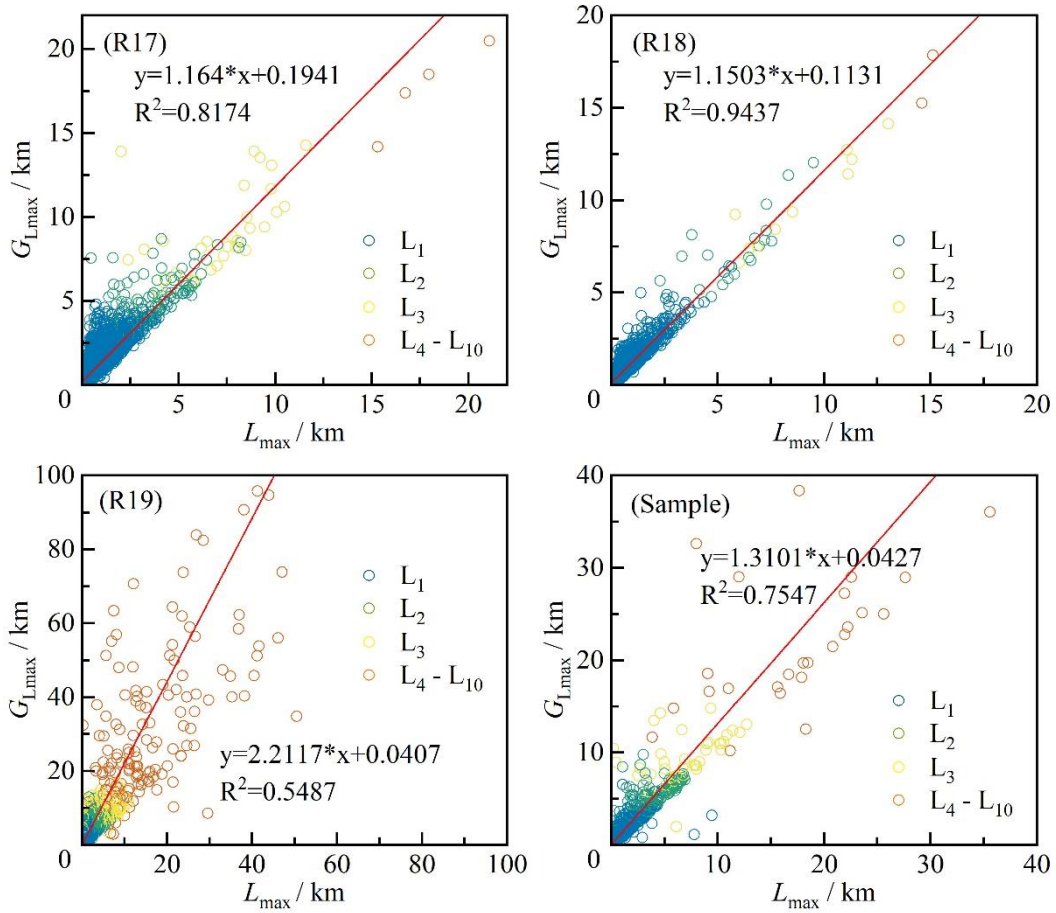
476
477 **Figure B1.** Linear regressions for different glacier regions between glacier length (G_{Lmax}) calculated
478 in this study and glacier length (L_{max}) calculated by Machguth and Huss (2014).
479

480

481

482

483

484

485

486

487

488

489
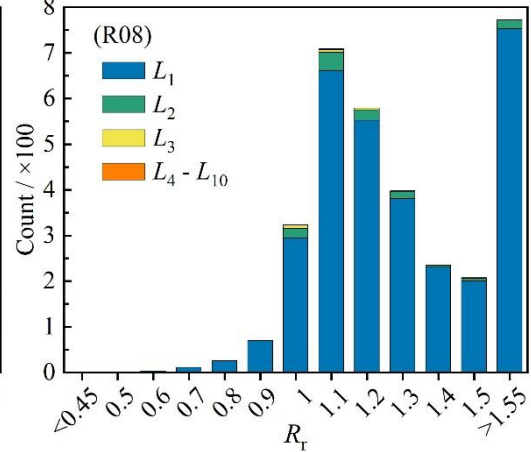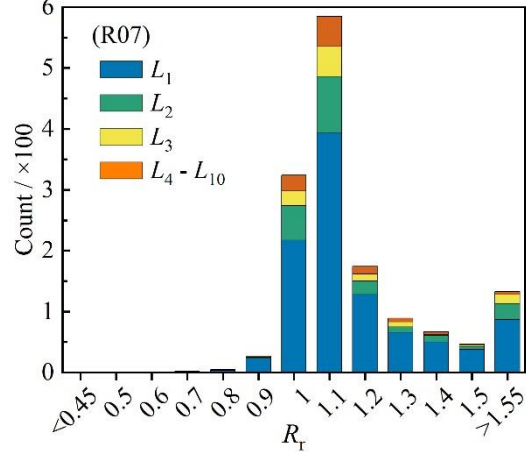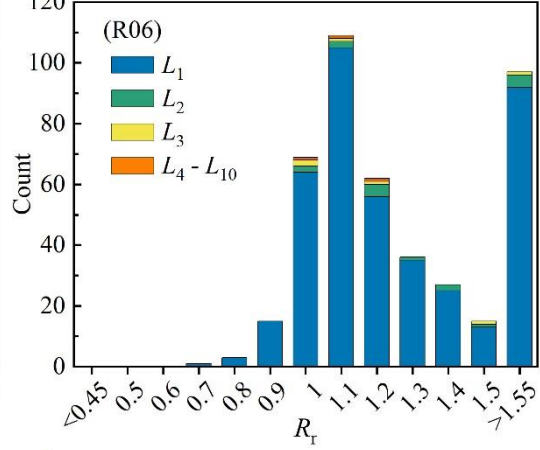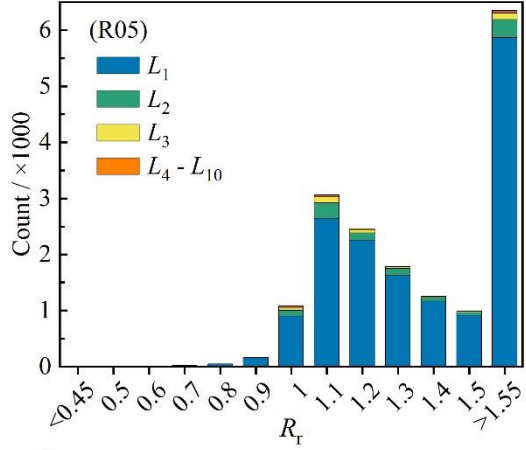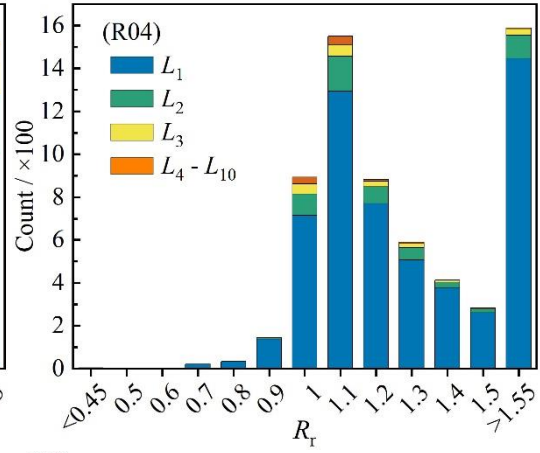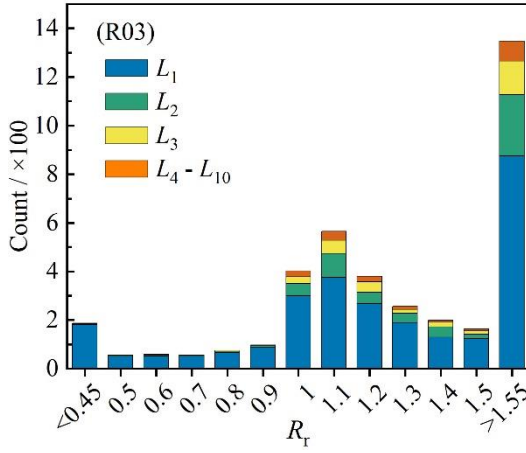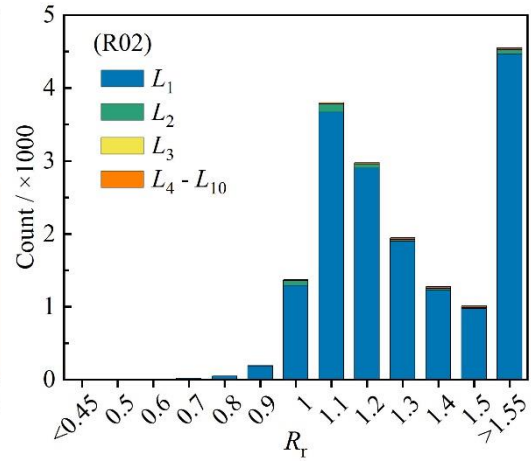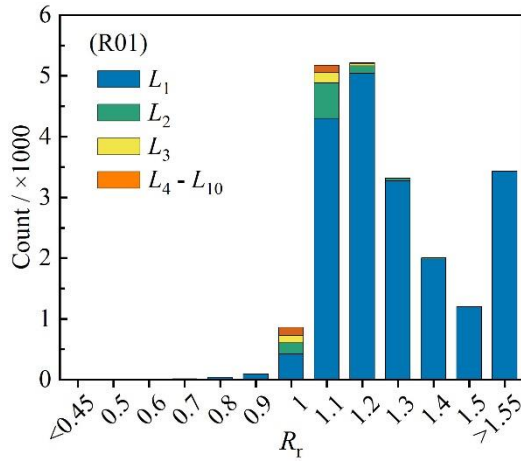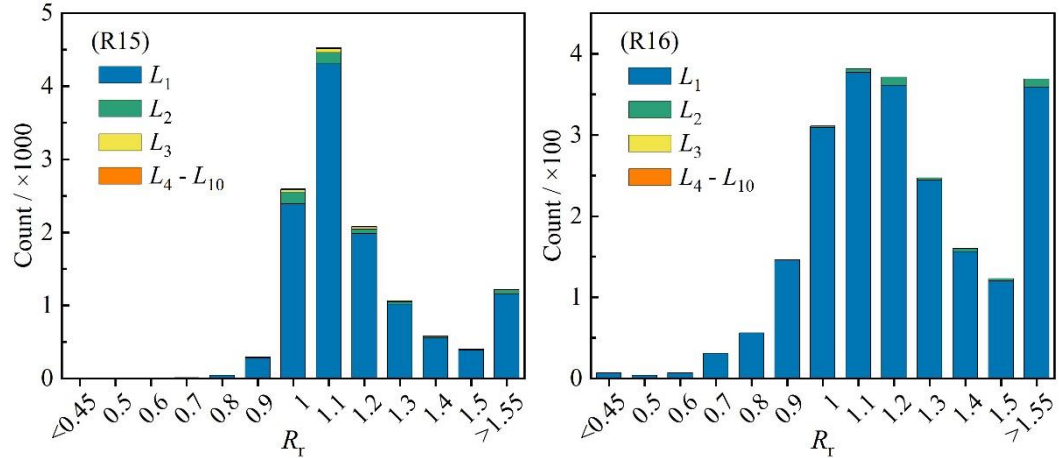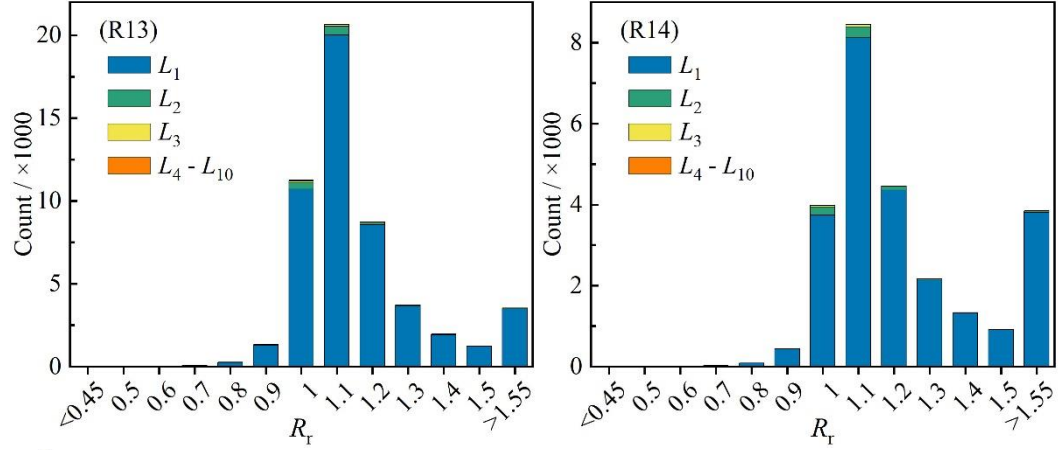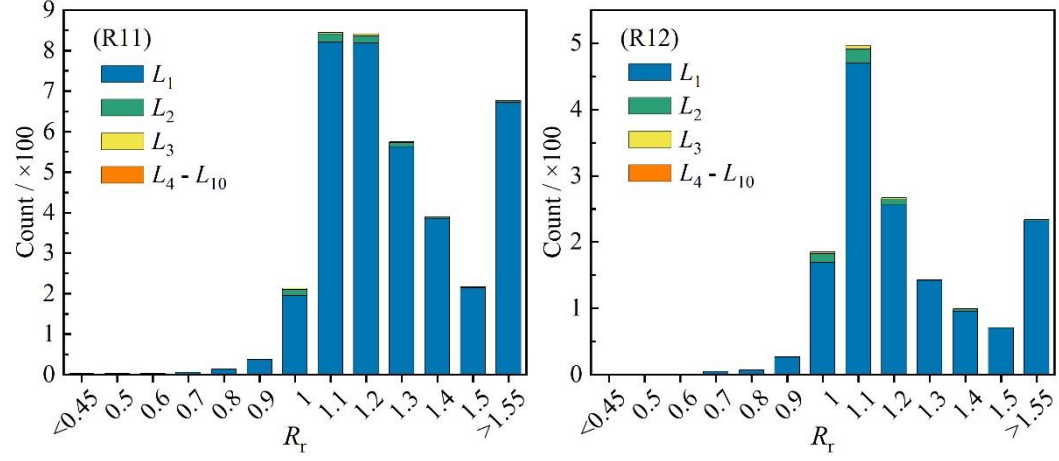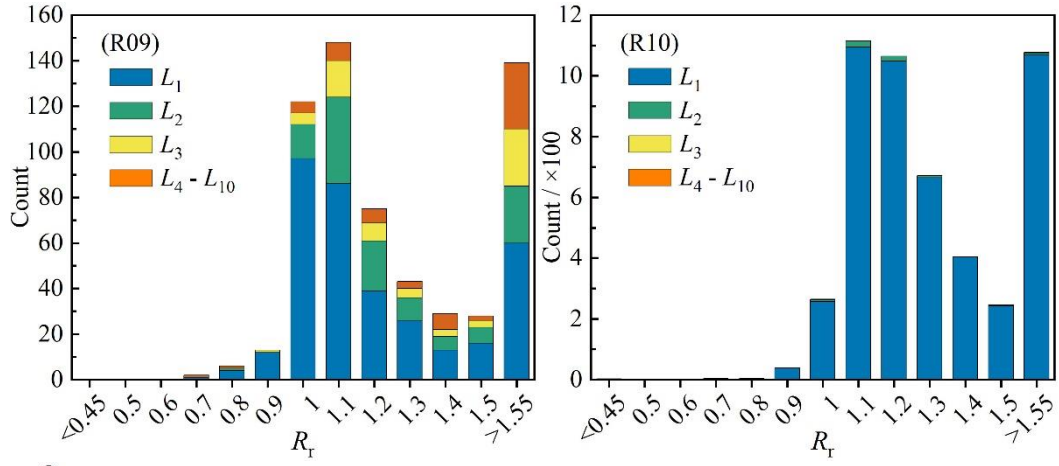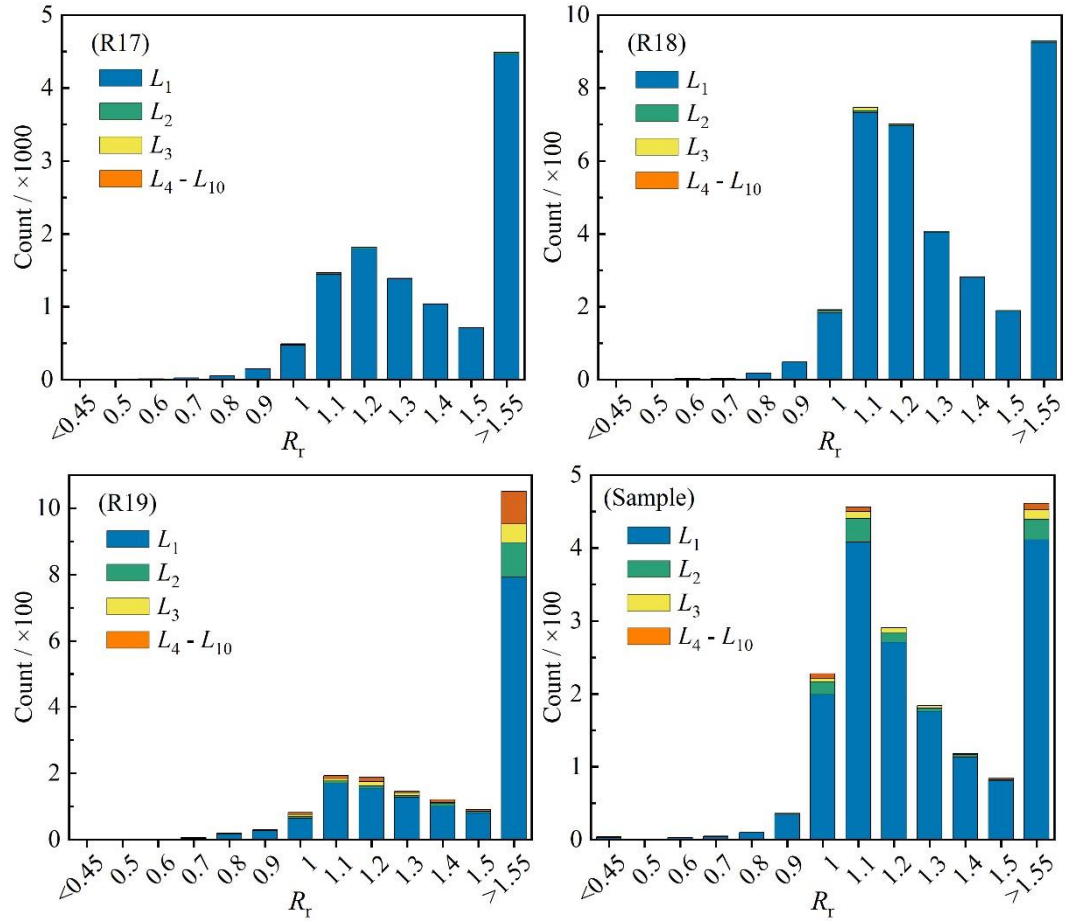
490 **Figure B2.** Histograms of the length ratio (R_r, G_{Lmax}/L_{max}) of distinct glacier grades in glacier-
491 covered regions and all samples.

492

493

494

495

496

497

498

499

500

501

502
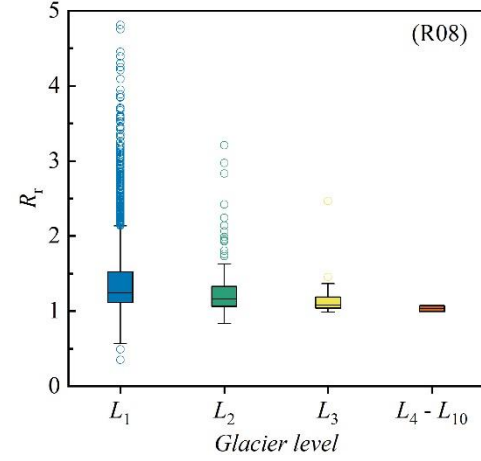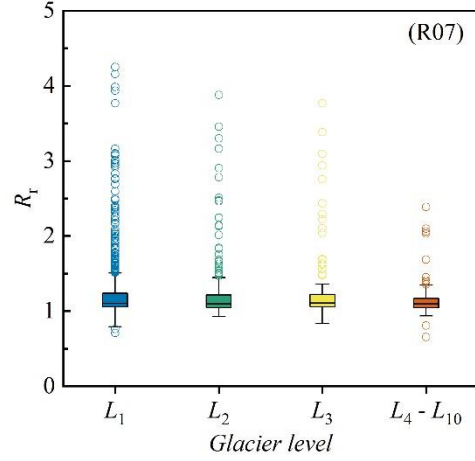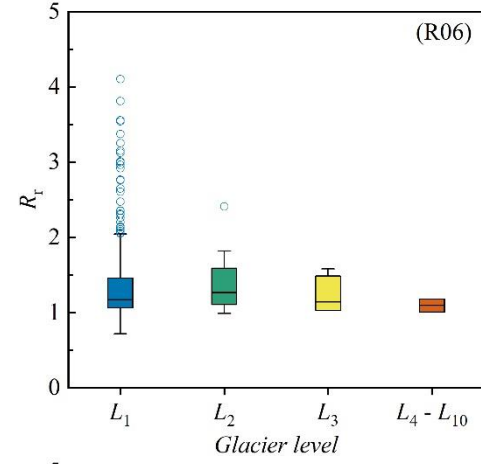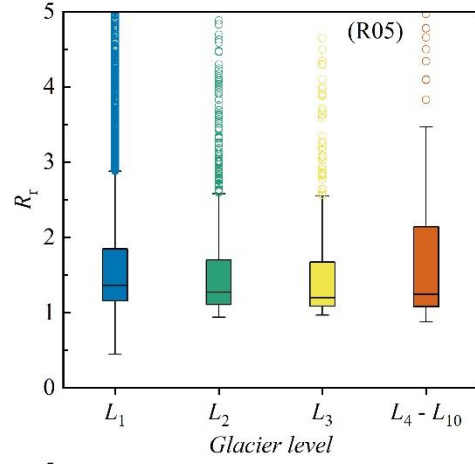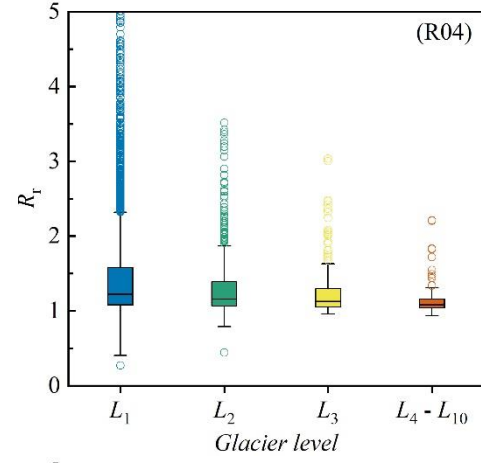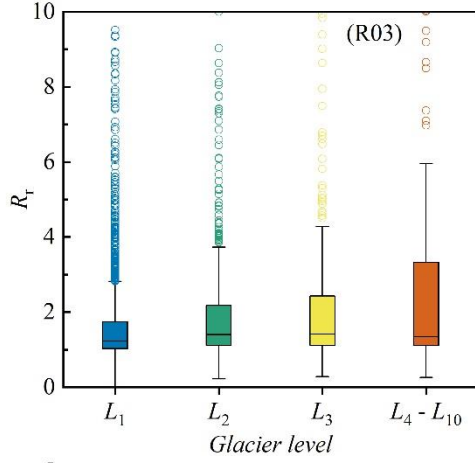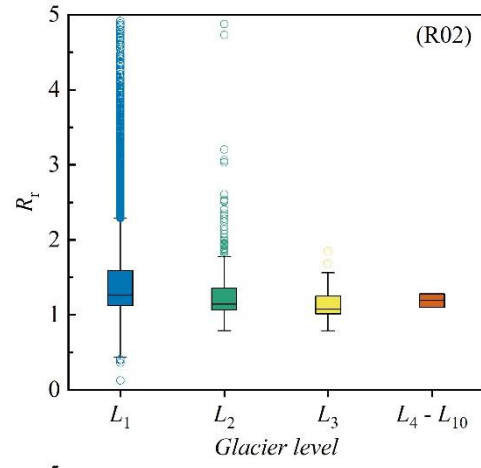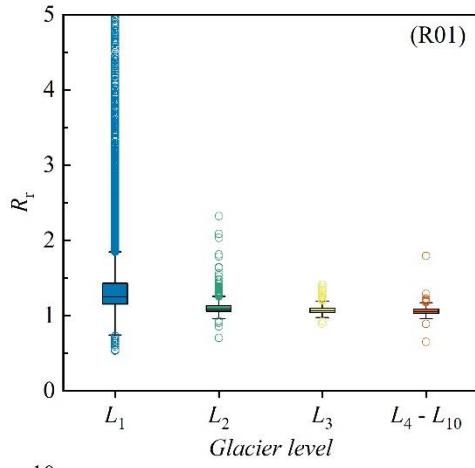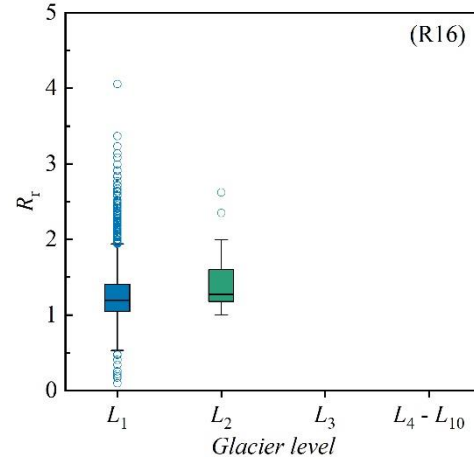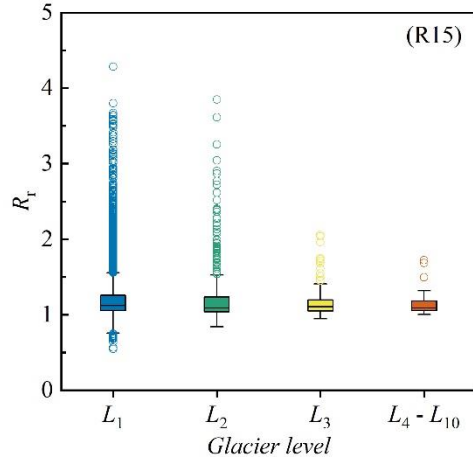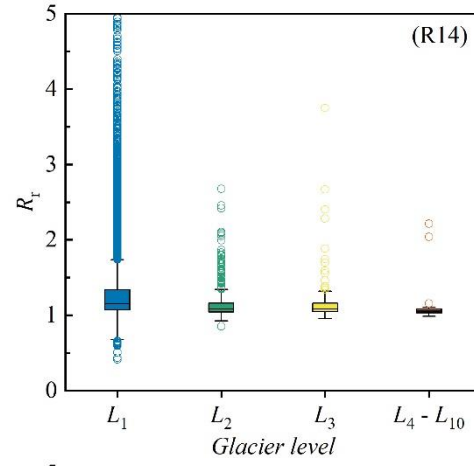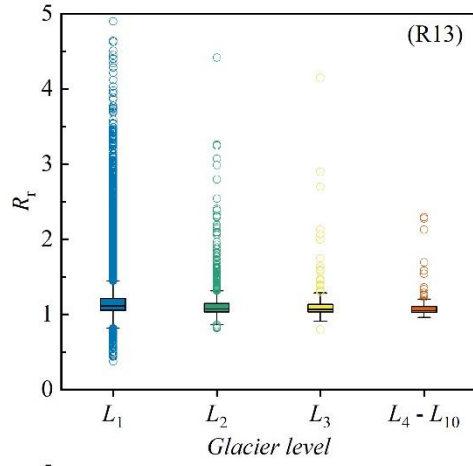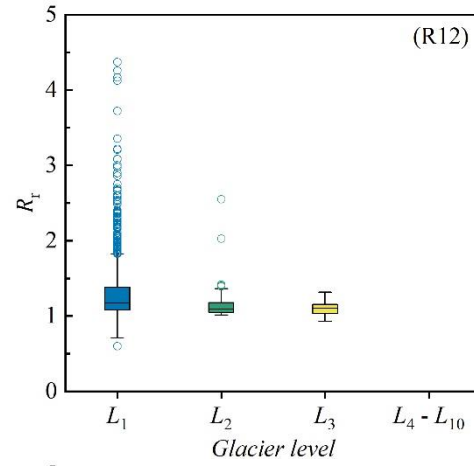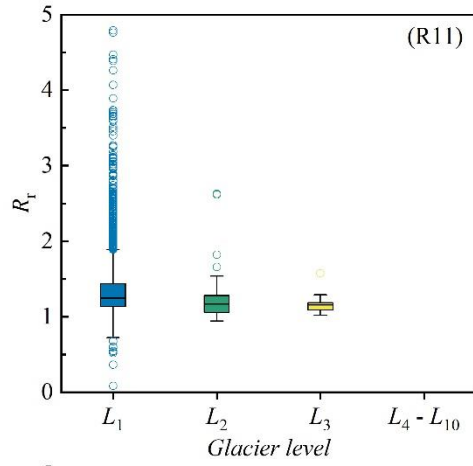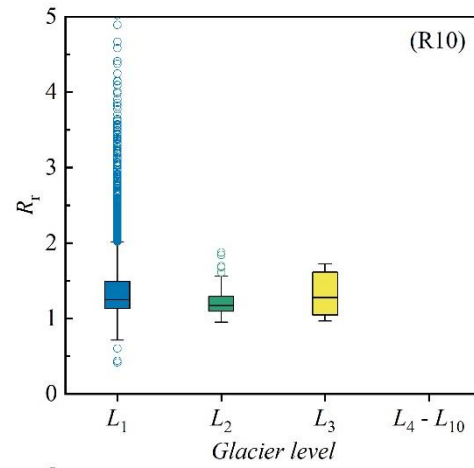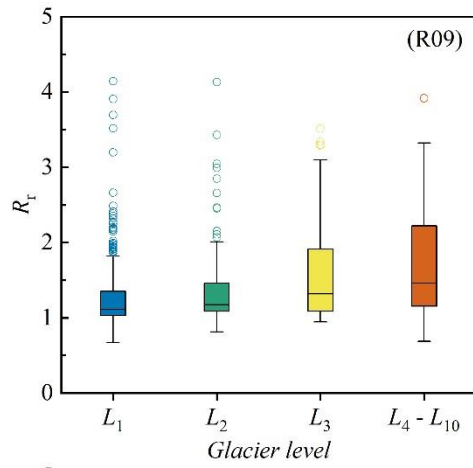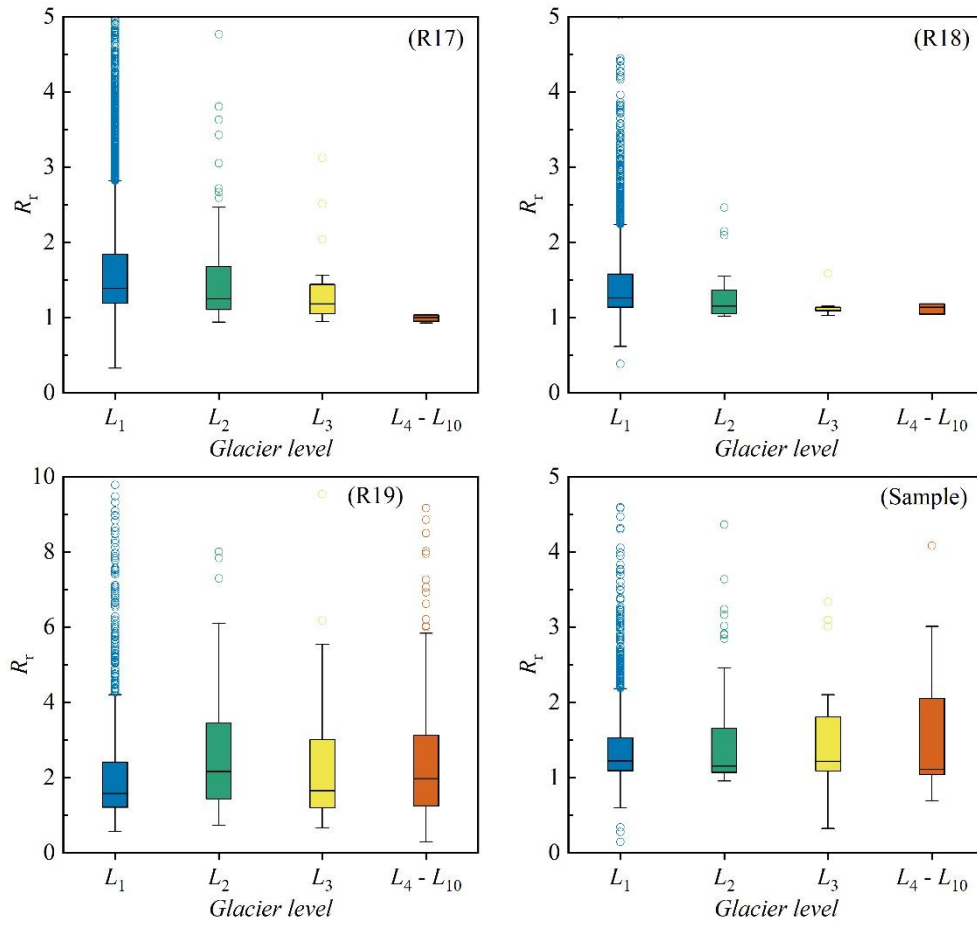
Figure B3. Box plots of length ratio (R_r, G_{Lmax}/L_{max}) of glaciers of distinct grades in every glacier-
covered region and whole sample.

505

Supplement.

The Supplement consists of three parts: (1) 'GlacierCenterlines_Py27' (version 5.2.1), the updated automatic extraction tool of glacier centerlines in this study, which fixed some defects compared with version 5.2.0 (https://doi.org/10.5194/tc-151955-2021-supplement). (2) 'Other_parameters_T1.txt' is the parameter file for extracting the global glacier centerlines. (3) The parameter files (format: *.prj) of the projected coordinate systems (Albers) of 19 glacier regions used in this study, which can be viewed with a text viewer and directly imported into ArcGIS software for further analysis.

Author contributions.

All authors contributed to writing and editing the manuscript. DZ processed the data, performed all calculations, created all figures, and wrote most of the manuscript. SZ contributed significantly to the development of the analyses, figures, and writing. XY contributed to the development of the data production strategy and writing. GZ and WL contributed to the initial data production. SW participated in writing Chapter 4.

Competing interests.

The authors declare that they have no conflict of interest.

Acknowledgments.

We thank editors, two reviewers and community scholars for their valuable comments that improved the manuscript. The authors would especially like to thank GLIMS for releasing the RGI v6.0 (http://www.glims.org/RGI/randolph.html, last accessed: November 15, 2021), LP DAAC for releasing the NASADEM (https://lpdaac.usgs.gov/news/release-nasadem-data-products/, last accessed: November 17, 2021), METI and NASA for jointly releasing the ASTER GDEM v3 (https://lpdaac.usgs.gov/news/nasa-and-meti-release-aster-global-dem-version-3/, last accessed: November 17, 2021), and the European Space Agency (ESA) for providing the Copernicus DEM (https://spacedata.copernicus.eu/web/cscda/cop-dem-faq, last accessed: November 17, 2021). This work would not have been possible without the support of open-access data.

Financial support.

This research was funded by the Second Tibetan Plateau Scientific Expedition and Research Program (STEP) (grant number: 2019QZKK020109) and China National Natural Science Foundation (grant numbers: 41730751, 42171124).

References

Abrams, M., Crippen, R., and Fujisada, H.: ASTER Global Digital Elevation Model (GDEM) and ASTER Global Water Body Dataset (ASTWBD), Remote Sensing, 12, https://doi.org/10.3390/rs12071156, 2020.

Aciego, S. M., Stevenson, E. I., and Arendt, C. A.: Climate versus geological controls on glacial meltwater micronutrient production in southern Greenland, Earth and Planetary Science Letters, 424, 51-58, https://doi.org/10.1016/j.epsl.2015.05.017, 2015.

Carabajal, C. C. and Boy, J. P.: Evaluation of Aster Gdem V3 Using Icesat Laser Altimetry, ISPRS - International Archives of the Photogrammetry, Remote Sensing and Spatial Information Sciences,

550   XLI-B4, 117-124, https://doi.org/10.5194/isprsarchives-XLI-B4-117-2016, 2016.

551 Carrera-Hernández, J. J.: Not all DEMs are equal: An evaluation of six globally available 30 m resolution
552   DEMs with geodetic benchmarks and LiDAR in Mexico, Remote Sensing of Environment, 261,
553   https://doi.org/10.1016/j.rse.2021.112474, 2021.

554 Cazenave, A.: Global sea-level budget 1993–present, Earth System Science Data, 10, 1551-1590,
555   https://doi.org/10.5194/essd-10-1551-2018, 2018.

556 Fan, Y., Ke, C.-Q., and Shen, X.: A new Greenland digital elevation model derived from ICESat-2 during
557   2018–2019, Earth System Science Data, 14, 781-794, https://doi.org/10.5194/essd-14-781-2022,
558   2022.

559 Farinotti, D., Huss, M., Fürst, J. J., Landmann, J., Machguth, H., Maussion, F., and Pandit, A.: A
560   consensus estimate for the ice thickness distribution of all glaciers on Earth, Nature Geoscience, 12,
561   168-173, https://doi.org/10.1038/s41561-019-0300-3, 2019.

562 Farr, T. G., Rosen, P. A., Caro, E., Crippen, R., Duren, R., Hensley, S., Kobrick, M., Paller, M., Rodriguez,
563   E., Roth, L., Seal, D., Shaffer, S., Shimada, J., Umland, J., Werner, M., Oskin, M., Burbank, D., and
564   Alsdorf, D.: The Shuttle Radar Topography Mission, Reviews of Geophysics, 45, 1-33,
565   https://doi.org/10.1029/2005rg000183, 2007.

566 Franke, S., Jansen, D., Binder, T., Paden, J. D., Dörr, N., Gerber, T. A., Miller, H., Dahl-Jensen, D., Helm,
567   V., Steinhage, D., Weikusat, I., Wilhelms, F., and Eisen, O.: Airborne ultra-wideband radar sounding
568   over the shear margins and along flow lines at the onset region of the Northeast Greenland Ice
569   Stream, Earth System Science Data, 14, 763-779, https://doi.org/10.5194/essd-14-763-2022, 2022.

570 Gao, Y. P., Yao, X. J., Liu, S. Y., Qi, M. M., Gong, P., An, L. N., Li, X. F., and Duan, H. Y.: Methods and
571   future trend of ice volume calculation of glacier, Arid Land Geography, 41, 1204-1213,
572   https://doi.org/10.12118/j.issn.1000-6060.2018.06.08, 2018.

573 Hansen, K., Hasenstab, K., and Schwartzman, A.: Estimating Mountain Glacier Flowlines by Local
574   Linear Regression Gradient Descent, IEEE Transactions on Geoscience and Remote Sensing, 59,
575   10022-10034, https://doi.org/10.1109/tgrs.2020.3035513, 2020.

576 Heid, T. and Kääb, A.: Repeat optical satellite images reveal widespread and long term decrease in land-
577   terminating glacier speeds, The Cryosphere, 6, 467-478, https://doi.org/10.5194/tc-6-467-2012,
578   2012.

579 Herla, F., Roe, G. H., and Marzeion, B.: Ensemble statistics of a geometric glacier length model, Annals
580   of Glaciology, 58, 130-135, https://doi.org/10.1017/aog.2017.15, 2017.

581 Herreid, S. and Pellicciotti, F.: The state of rock debris covering Earth's glaciers, Nature Geoscience, 13,
582   621-627, https://doi.org/10.1038/s41561-020-0615-0, 2020.

583 Howat, I. M., Porter, C., Smith, B. E., Noh, M.-J., and Morin, P.: The Reference Elevation Model of
584   Antarctica, The Cryosphere, 13, 665-674, https://doi.org/10.5194/tc-13-665-2019, 2019.

585 Hugonnet, R., McNabb, R., Berthier, E., Menounos, B., Nuth, C., Girod, L., Farinotti, D., Huss, M.,
586   Dussaillant, I., Brun, F., and Kaab, A.: Accelerated global glacier mass loss in the early twenty-first
587   century, Nature, 592, 726-731, https://doi.org/10.1038/s41586-021-03436-z, 2021.

588 Immerzeel, W. W., Lutz, A. F., Andrade, M., Bahl, A., Biemans, H., Bolch, T., Hyde, S., Brumby, S.,
589   Davies, B. J., Elmore, A. C., Emmer, A., Feng, M., Fernández, A., Haritashya, U., Kargel, J. S.,
590   Koppes, M., Kraaijenbrink, P. D. A., Kulkarni, A. V., Mayewski, P. A., Nepal, S., Pacheco, P., Painter,
591   T. H., Pellicciotti, F., Rajaram, H., Rupper, S., Sinisalo, A., Shrestha, A. B., Viviroli, D., Wada, Y.,
592   Xiao, C., Yao, T., and Baillie, J. E. M.: Importance and vulnerability of the world's water towers,
593   Nature, 577, 364-369, https://doi.org/10.1038/s41586-019-1822-y, 2019.

Ji, Q., Yang, T.-b., He, Y., Qin, Y., Dong, J., and Hu, F.-s.: A simple method to extract glacier length based on Digital Elevation Model and glacier boundaries for simple basin type glacier, Journal of Mountain Science, 14, 1776-1790, https://doi.org/10.1007/s11629-016-4243-5, 2017.

Kääb, A., Jacquemart, M., Gilbert, A., Leinss, S., Girod, L., Huggel, C., Falaschi, D., Ugalde, F., Petrakov, D., Chernomorets, S., Dokukin, M., Paul, F., Gascoin, S., Berthier, E., and Kargel, J. S.: Sudden large-volume detachments of low-angle mountain glaciers – more frequent than thought?, The Cryosphere, 15, 1751-1785, https://doi.org/10.5194/tc-15-1751-2021, 2021.

Kienholz, C., Hock, R., and Arendt, A. A.: A new semi-automatic approach for dividing glacier complexes into individual glaciers, Journal of Glaciology, 59, 925-937, https://doi.org/10.3189/2013JoG12J138, 2013.

Kienholz, C., Rich, J. L., Arendt, A. A., and Hock, R.: A new method for deriving glacier centerlines applied to glaciers in Alaska and northwest Canada, The Cryosphere, 8, 503-519, https://doi.org/10.5194/tc-8-503-2014, 2014.

Le Bris, R. and Paul, F.: An automatic method to create flow lines for determination of glacier length: A pilot study with Alaskan glaciers, Computers & Geosciences, 52, 234-245, https://doi.org/10.1016/j.cageo.2012.10.014, 2013.

Le Moine, N. and Gsell, P.-S.: A graph-based approach to glacier flowline extraction: An application to glaciers in Switzerland, Computers & Geosciences, 85, 91-101, https://doi.org/10.1016/j.cageo.2015.09.010, 2015.

Leclercq, P. W. and Oerlemans, J.: Global and hemispheric temperature reconstruction from glacier length fluctuations, Climate Dynamics, 38, 1065-1079, https://doi.org/10.1007/s00382-011-1145-7, 2011.

Leclercq, P. W., Oerlemans, J., Basagic, H. J., Bushueva, I., Cook, A. J., and Le Bris, R.: A data set of worldwide glacier length fluctuations, The Cryosphere, 8, 659-672, https://doi.org/10.5194/tc-8-659-2014, 2014.

Li, H., Ng, F., Li, Z., Qin, D., and Cheng, G.: An extended "perfect-plasticity" method for estimating ice thickness along the flow line of mountain glaciers, Journal of Geophysical Research: Earth Surface, 117, n/a-n/a, https://doi.org/10.1029/2011jf002104, 2012.

Li, X., Ding, Y., Hood, E., Raiswell, R., Han, T., He, X., Kang, S., Wu, Q., Yu, Z., Mika, S., Liu, S., and Li, Q.: Dissolved Iron Supply from Asian Glaciers: Local Controls and a Regional Perspective, Global Biogeochemical Cycles, 33, 1223-1237, https://doi.org/10.1029/2018gb006113, 2019.

Li, Y., Li, F., Shangguan, D., and Ding, Y.: A new global gridded glacier dataset based on the Randolph Glacier Inventory version 6.0, Journal of Glaciology, 67, 773-776, https://doi.org/10.1017/jog.2021.28, 2021.

Lüthi, M. P., Bauder, A., and Funk, M.: Volume change reconstruction of Swiss glaciers from length change data, Journal of Geophysical Research, 115, https://doi.org/10.1029/2010jf001695, 2010.

Machguth, H. and Huss, M.: The length of the world's glaciers – a new approach for the global calculation of center lines, The Cryosphere, 8, 1741-1755, https://doi.org/10.5194/tc-8-1741-2014, 2014.

Mankoff, K. D., Fettweis, X., Langen, P. L., Stendel, M., Kjeldsen, K. K., Karlsson, N. B., Noël, B., van den Broeke, M. R., Solgaard, A., Colgan, W., Box, J. E., Simonsen, S. B., King, M. D., Ahlstrøm, A. P., Andersen, S. B., and Fausto, R. S.: Greenland ice sheet mass balance from 1840 through next week, Earth System Science Data, 13, 5001-5025, https://doi.org/10.5194/essd-13-5001-2021, 2021.

Maussion, F., Butenko, A., Champollion, N., Dusch, M., Eis, J., Fourteau, K., Gregor, P., Jarosch, A. H., Landmann, J., Oesterle, F., Recinos, B., Rothenpieler, T., Vlug, A., Wild, C. T., and Marzeion, B.:

The Open Global Glacier Model (OGGM) v1.1, Geoscientific Model Development, 12, 909-931, https://doi.org/10.5194/gmd-12-909-2019, 2019.

Melkonian, A. K., Willis, M. J., and Pritchard, M. E.: Satellite-derived volume loss rates and glacier speeds for the Juneau Icefield, Alaska, Journal of Glaciology, 60, 743-760, https://doi.org/10.3189/2014JoG13J181, 2017.

Noel, B., Jakobs, C. L., van Pelt, W. J. J., Lhermitte, S., Wouters, B., Kohler, J., Hagen, J. O., Luks, B., Reijmer, C. H., van de Berg, W. J., and van den Broeke, M. R.: Low elevation of Svalbard glaciers drives high mass loss variability, Nat Commun, 11, 4597, https://doi.org/10.1038/s41467-020-18356-1, 2020.

Oerlemans, J.: A flowline model for Nigardsbreen, Norway: projection of future glacier length based on dynamic calibration with the historic record, Annals of Glaciology, 24, 382-389, https://doi.org/10.1017/S0260305500012489 1997.

Pfeffer, W. T., Arendt, A. A., Bliss, A., Bolch, T., Cogley, J. G., Gardner, A. S., Hagen, J.-O., Hock, R., Kaser, G., Kienholz, C., Miles, E. S., Moholdt, G., Mölg, N., Paul, F., Radić, V., Rastner, P., Raup, B. H., Rich, J., and Sharp, M. J.: The Randolph Glacier Inventory: a globally complete inventory of glaciers, Journal of Glaciology, 60, 537-552, https://doi.org/10.3189/2014JoG13J176, 2014.

Pritchard, H. D.: Asia's shrinking glaciers protect large populations from drought stress, Nature, 569, 649-654, https://doi.org/10.1038/s41586-019-1240-1, 2019.

Radić, V. and Hock, R.: Regional and global volumes of glaciers derived from statistical upscaling of glacier inventory data, Journal of Geophysical Research, 115, https://doi.org/10.1029/2009jf001373, 2010.

RGI Consortium: Randolph Glacier Inventory – A Dataset of Global Glacier Outlines: Version 6.0: Technical Report, Global Land Ice Measurements from Space, Colorado, USA, 10.7265/N5-RGI-60, 2017.

Scherler, D., Wulf, H., and Gorelick, N.: Global Assessment of Supraglacial Debris-Cover Extents, Geophysical Research Letters, 45, 11,798-711,805, https://doi.org/10.1029/2018gl080158, 2018.

Schiefer, E., Menounos, B., and Wheate, R.: An inventory and morphometric analysis of British Columbia glaciers, Canada, Journal of Glaciology, volume 54, 551-560, 2008.

Shukla, A., Garg, S., Mehta, M., Kumar, V., and Shukla, U. K.: Temporal inventory of glaciers in the Suru sub-basin, western Himalaya: impacts of regional climate variability, Earth System Science Data, 12, 1245-1265, https://doi.org/10.5194/essd-12-1245-2020, 2020.

Shukla, T. and Sen, I. S.: Preparing for floods on the Third Pole, Science, 372, 232-234, https://doi.org/10.1126/science.abh3558, 2021.

Solgaard, A., Kusk, A., Merryman Boncori, J. P., Dall, J., Mankoff, K. D., Ahlstrøm, A. P., Andersen, S. B., Citterio, M., Karlsson, N. B., Kjeldsen, K. K., Korsgaard, N. J., Larsen, S. H., and Fausto, R. S.: Greenland ice velocity maps from the PROMICE project, Earth System Science Data, 13, 3491-3512, https://doi.org/10.5194/essd-13-3491-2021, 2021.

Sommer, C., Malz, P., Seehaus, T. C., Lippl, S., Zemp, M., and Braun, M. H.: Rapid glacier retreat and downwasting throughout the European Alps in the early 21(st) century, Nat Commun, 11, 3209, https://doi.org/10.1038/s41467-020-16818-0, 2020.

Stuart-Smith, R. F., Roe, G. H., Li, S., and Allen, M. R.: Increased outburst flood hazard from Lake Palcacocha due to human-induced glacier retreat, Nature Geoscience, 14, 85-90, https://doi.org/10.1038/s41561-021-00686-4, 2021.

Sugiyama, S., Bauder, A., Zahno, C., and Funk, M.: Evolution of Rhonegletscher, Switzerland, over the

past 125 years and in the future : application of an improved flowline model, Annals of Glaciology, 46, 268-274, 2007.

Thogersen, K., Gilbert, A., Schuler, T. V., and Malthe-Sorenssen, A.: Rate-and-state friction explains glacier surge propagation, Nat Commun, 10, 2823, https://doi.org/10.1038/s41467-019-10506-4, 2019.

Uuemaa, E., Ahi, S., Montibeller, B., Muru, M., and Kmoch, A.: Vertical Accuracy of Freely Available Global Digital Elevation Models (ASTER, AW3D30, MERIT, TanDEM-X, SRTM, and NASADEM), Remote Sensing, 12, https://doi.org/10.3390/rs12213482, 2020.

Vargo, L. J., Anderson, B. M., Dadić, R., Horgan, H. J., Mackintosh, A. N., King, A. D., and Lorrey, A. M.: Anthropogenic warming forces extreme annual glacier mass loss, Nature Climate Change, 10, 856-861, https://doi.org/10.1038/s41558-020-0849-2, 2020.

Winsvold, S. H., Andreassen, L. M., and Kienholz, C.: Glacier area and length changes in Norway from repeat inventories, The Cryosphere, 8, 1885-1903, https://doi.org/10.5194/tc-8-1885-2014, 2014.

Wu, K., Liu, S., Jiang, Z., Liu, Q., Zhu, Y., Yi, Y., Xie, F., Ahmad Tahir, A., and Saifullah, M.: Quantification of glacier mass budgets in the Karakoram region of Upper Indus Basin during the early twenty-first century, Journal of Hydrology, 603, https://doi.org/10.1016/j.jhydrol.2021.127095, 2021.

Xia, W.: An Automatic Extraction Method of Glacier Length Based on Voronoi Algorithm - A Pilot Study in the Sanjiangyuan Region, College of Urban and Environmental Science, Northwest University, Xi'an, Shannxi, 2020.

Yang, B. Y., Zhang, L. X., Gao, Y., Xiang, Y., Mou, N. X., and Suo, L. D. B.: An integrated method of glacier length extraction based on Gaofen satellite data, Journal of Glaciology and Geocryology, 38, 1615-1623, https://doi.org/10.7522/j.issn.1000-0240.2016.0189, 2016.

Yao, X. J., Liu, S. Y., Zhu, Y., Gong, P., An, L. N., and Li, X. F.: Design and implementation of an automatic method for deriving glacier centerlines based on GIS, Journal of Glaciology and Geocryology, 37, 1563-1570, https://doi.org/10.7522/j.issn.1000-0240.2015.0173, 2015.

Zemp, M., Huss, M., Thibert, E., Eckert, N., McNabb, R., Huber, J., Barandun, M., Machguth, H., Nussbaumer, S. U., Gartner-Roer, I., Thomson, L., Paul, F., Maussion, F., Kutuzov, S., and Cogley, J. G.: Global glacier mass changes and their contributions to sea-level rise from 1961 to 2016, Nature, 568, 382-386, https://doi.org/10.1038/s41586-019-1071-0, 2019.

Zhang, B., Wang, Z., An, J., Liu, T., and Geng, H.: A 30-year monthly 5 km gridded surface elevation time series for the Greenland Ice Sheet from multiple satellite radar altimeters, Earth System Science Data, 14, 973-989, https://doi.org/10.5194/essd-14-973-2022, 2022.

Zhang, D. and Zhang, S.: A new global dataset of mountain glacier centerline and length, Science Data Bank, https://doi.org/10.11922/sciencedb.01643, 2022.

Zhang, D., Yao, X., Duan, H., Liu, S., Guo, W., Sun, M., and Li, D.: A new automatic approach for extracting glacier centerlines based on Euclidean allocation, The Cryosphere, 15, 1955-1973, https://doi.org/10.5194/tc-15-1955-2021, 2021.

Zheng, G., Allen, S. K., Bao, A., Ballesteros-Cánovas, J. A., Huss, M., Zhang, G., Li, J., Yuan, Y., Jiang, L., Yu, T., Chen, W., and Stoffel, M.: Increasing risk of glacial lake outburst floods from future Third Pole deglaciation, Nature Climate Change, 11, 411-417, https://doi.org/10.1038/s41558-021-01028-3, 2021.

Zhou, S., Yao, X., Zhang, D., Zhang, Y., Liu, S., and Min, Y.: Remote Sensing Monitoring of Advancing and Surging Glaciers in the Tien Shan, 1990–2019, Remote Sensing, 13,

726 https://doi.org/10.3390/rs13101973, 2021a.

727 Zhou, Y., Li, X., Zheng, D., Li, Z., An, B., Wang, Y., Jiang, D., Su, J., and Cao, B.: The joint driving
728   effects of climate and weather changes caused the Chamoli glacier-rock avalanche in the high
729   altitudes of the India Himalaya, Science China Earth Sciences, 64, 1909-1921,
730   https://doi.org/10.1007/s11430-021-9844-0, 2021b.

731